DIRECT MEASUREMENT OF DISSIPATIVE FORCES IN SUPERCONDUCTING BSCCO

by

ELIZABETH EILEEN JUDGE, B.S.

DISSERTATION

Presented to the Faculty of the Graduate School of
The University of Texas at Austin
in Partial Fulfillment
of the Requirements
for the Degree of

DOCTOR OF PHILOSOPHY

THE UNIVERSITY OF TEXAS AT AUSTIN
August 2001

UMI Number: 3035957

ProQuest Information and Learning Company
300 North Zeeb Road
PO Box 1346
Ann Arbor, MI 48106-1346

The Dissertation Committee for Elizabeth Eileen Judge
Certifies that this is the approved version of the following dissertation:

DIRECT MEASUREMENT OF DISSIPATIVE FORCES IN SUPERCONDUCTING BSCCO

Committee:

John T. Markert, Supervisor

John B. Goodenough

Qian Niu

Alejandro de Lozanne

Jack Swift

Acknowledgements

I would like to thank Dr. Markert in particular for his support and understanding. I would also like to thank the numerous other faculty members who have acted as advisors to me both officially and unofficially. I would like to thank all of my friends. Without their friendship and homework help, I would have surely have been left floundering. I would like especially to thank my family. They have provided me with many forms of support throughout my many years of university work.

DIRECT MEASUREMENT OF DISSIPATIVE FORCES IN SUPERCONDUCTING BSCCO

Publication No. ____________________

Elizabeth Eileen Judge, Ph.D.
The University of Texas at Austin, 2001

Supervisor: John T. Markert

We report direct measurement of the viscous force on moving vortices in single-crystal, high-T_c superconductors using high-Q, double-torsional, single-crystal silicon, mechanical oscillators. Our technique applies a magnetic field through the center of the crystal, avoiding edge pinning effects, and drives the vortices by physically oscillating the magnet, avoiding the necessity for leads. We find for the high-T_c superconductor $Bi_2Sr_2CaCu_2O_8$ the value of the dissipation coefficient per vortex per unit length at 77 K is $\eta = 5.8 \times 10^{-7}$ g/cm-s.

Table of Contents

Appendices

List of Figures

List of Tables

Chapter 1

Introduction

Superconductivity was first discovered by Kamerlingh Onnes in 1911 [1]. At a critical temperature, T_c, a superconducting sample will undergo a sudden phase transition from a state of finite resistivity (normal state) to a state of zero resistivity (superconducting state). Some seventy years later, copper-oxide compounds were discovered to exhibit high-temperature superconductivity [2]. In the meantime, significant work, both experimental and theoretical, was being done in an attempt to understand this new phenomenon. Both thermodynamics and quantum mechanics were called upon to develop a theoretical picture. For the high-temperature materials, the quantum picture is far from clear. The thermodynamic picture, in the form of Ginsburg-Landau theory, is much more complete.

1.1 Characteristics of Superconductivity

The two hallmarks of superconductivity are infinite conductivity and perfect diamagnetism. The first refers to the absence of measurable resistivity. The second refers to the expulsion of a magnetic field from the inside of a superconductor. Note that setting the conductivity to infinity in Maxwell's equations will not result in a description of a perfect diamagnet. A perfect conductor would be expected to *exclude* a magnetic field. A superconductor goes one step further and *expels* any magnetic field which is already inside. This is known as the Meissner effect. This expulsion can be explained thermodynamically by relating the free energy difference between the superconducting and normal states to a critical field H_c which will destroy the superconductivity. More precisely,

$$f_n(T) - f_s(T) = \frac{H_c^2(T)}{8\pi} \tag{1.1}$$

where $f_n(T)$ is the free energy of the normal state, $f_s(T)$ is the free energy of the superconducting state.

Infinite conductivity and perfect diamagnetism are described by the London equations [3]

$$\vec{E} = \frac{\partial}{\partial t}(\Lambda \vec{J}_s) \tag{1.2}$$

$$\vec{H} = -c\nabla \times (\Lambda \vec{J}_s) \tag{1.3}$$

where

$$\Lambda = \frac{4\pi\lambda_L^2}{c^2} = \frac{m}{n_s e^2} \tag{1.4}$$

is a phenomenological parameter.

The second London equation can be combined with the Maxwell equation

$$\nabla \times \vec{H} = \frac{4\pi \vec{J}}{c} \tag{1.5}$$

to find

$$\nabla^2 \vec{H} = \frac{\vec{H}}{\lambda_L^2} \tag{1.6}$$

This equation describes the screening of the interior of the superconductor from magnetic fields. The parameter λ_L is defined as the penetration depth of the field into the superconductor. It is the length scale over which the field and screening currents fall off. It is a characteristic of any given superconductor. Its value as T approaches zero is calculated from

$$\lambda_L(0) = \left(\frac{mc^2}{4\pi ne^2}\right)^{\frac{1}{2}}. \tag{1.7}$$

1.2 Ginsburg-Landau Theory

Ginsburg and Landau introduced a complex wave function which acts as an order parameter for the superconducting electrons [4]. The wave function is defined so that its square gives the local superconducting density found in the London equations:

$$n_s = |\psi(x)|^2 \tag{1.8}$$

They then used a variational principle applied to an assumed expansion of the free energy density to derive coupled differential equations in $\psi(x)$ and $\vec{A}$, the vector potential. The differential equation for ψ is analogous to the Schroedinger equation:

$$\frac{1}{2m^*}\left(\frac{\hbar}{i}\nabla - \frac{e^*}{c}\vec{A}\right)^2 \psi + \beta|\psi|^2\psi + \alpha(T)\psi = 0 \tag{1.9}$$

The basic postulate of GL theory is that if ψ is small, the free energy density f can expanded in powers of ψ [5]:

$$f = f_{n0} + \alpha|\psi|^2 + \frac{\beta}{2}|\psi|^4 + \frac{1}{2m}\left|\left(\frac{\hbar}{i}\nabla - \frac{e^*}{c}\vec{A}\right)\psi\right|^2 + \frac{h^2}{8\pi} \tag{1.10}$$

In these equations, m^* and e^* are the effective mass and effective charge, respectively, of the superconducting particles. α and β are coefficients the magnitude of which describes the superconducting effects. The parameter α changes sign at the transition temperature, T_c, while β is assumed to be constant in temperature [6].

Ginsburg-Landau (GL) theory expanded theoretical treatment of the superconducting state to areas which London theory could not handle. In particular, GL theory is able to treat spatially varying superconducting densities (n_s) and non-linear effects of fields strong enough to change n_s. GL theory is also able to handle the interface between normal and superconducting regions in the presence of fields $H \approx H_c$.

The superconducting order parameter also has a length scale associated with it, the cherence length, ξ. It is defined as

$$\xi(T) = \frac{\hbar}{|2m^*\alpha(T)|^{\frac{1}{2}}} \tag{1.11}$$

and characterizes the distance over which $\psi(\vec{r})$ can vary without significant change in energy. This length scale is a characteristic of a given superconductor.

The copper-oxide superconductors typically have length scales which depend on direction. This family of superconductors has a layered structure which is highly anisotropic. There are typically one or more copper-oxide layers within a unit cell, separated by one or more insulating layers. An example is in Fig. 1.1. Figure 1.1 represents three unit cells of $YBa_2Cu_3O_{6.95}$ (YBCO). The layered structure is clearly visible. The length scales ξ and λ are different in the ab direction than they are in the c direction.

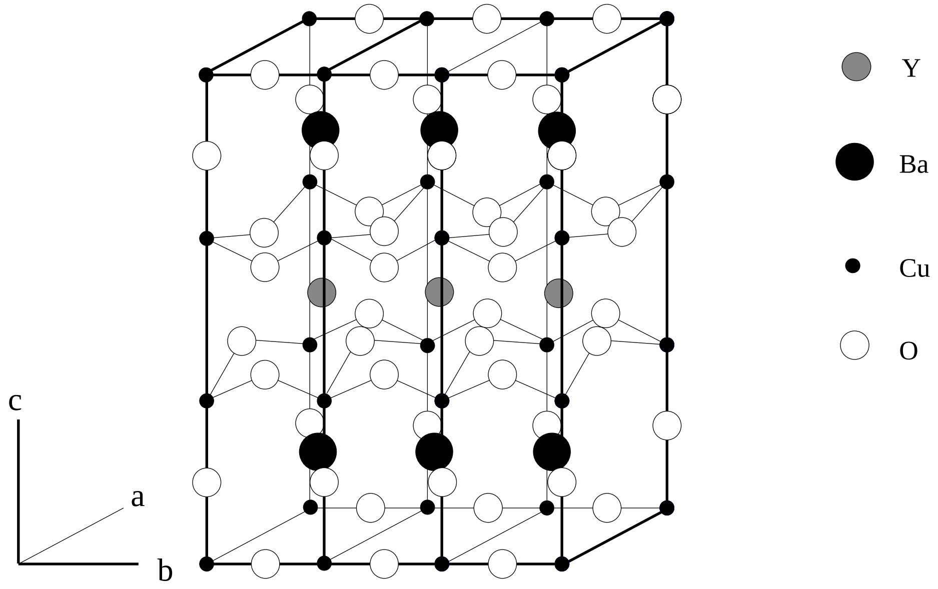

Figure 1.1: Structure of YBCO.

The ratio of the two length scales defines the Ginsburg-Landau parameter

$$\kappa = \frac{\lambda}{\xi}. \tag{1.12}$$

This dimensionless ratio is temperature independent near T_c. Its value divides superconductors in two types: type I and type II. The critical value is at $\kappa = 1/\sqrt{2}$. Values of ξ and λ are given in Table 1.1.

Table 1.1: Coherence length ξ, penetration depth λ, GL parameter κ, transition temperature T_c, and critical field H_c where flux first penetrates the sample at 0 K for selected superconducting materials. Data from [6, 7, 8].

Material	ξ (10^{-6} cm)	λ (10^{-6} cm)	κ	T_c (K)	H_c (G)[a]
Al	160	1.6	0.010	1.18	105
Pb	8.3	3.7	0.45	7.2	803
Nb	3.8	3.9	1.02	9.3	98
Nb_3Sn	0.34	16	47	18.5	28

[a] For the type II compounds, the value given for H_c is the value of H_{c1}.

1.3 The Vortex State

For $\lambda < \frac{1}{\sqrt{2}}\xi$, $\kappa < 1/\sqrt{2}$, and there will be a positive surface energy associated with the formation of a boundary between normal and superconducting domains. These are known as Type I superconductors. They have a single critical field, H_c, below which they exhibit perfect diamagnetism and above which superconductivity is destroyed. The H-T phase diagram is shown in Fig. 1.2.

For the reverse situation, $\lambda > \frac{1}{\sqrt{2}}\xi$ and $\kappa > 1/\sqrt{2}$, there is a negative surface energy associated with the formation of a boundary. In this situation, flux may penetrate the superconductor and form a normal region, giving rise to a boundary. This flux is quantized in units of

$$\Phi_o = \frac{hc}{2e} = 2.07 \times 10^{-7}\text{gauss-cm}^2. \tag{1.13}$$

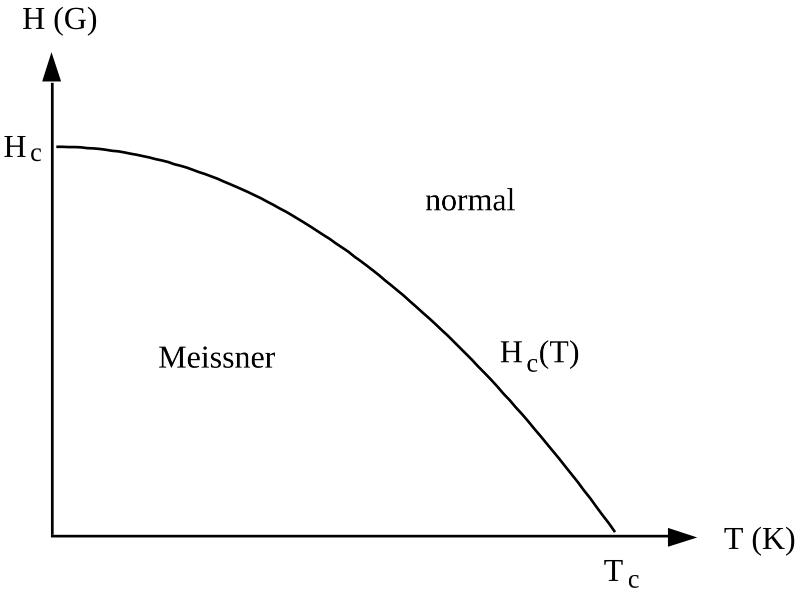

Figure 1.2: H-T phase diagram for a Type I superconductor.

A single quantum of flux (a flux line) is known as a vortex. These types of superconductors are known as type II superconductors. Type II superconductors have two critical fields. The lower field, H_{c1}, is the critical value at which flux lines may begin to penetrate. It can be calculated as [6]

$$H_{c1} = \frac{\Phi_o}{4\pi\lambda^2}\ln\frac{\lambda}{\xi}. \tag{1.14}$$

Below this value, the superconductor exhibits perfect diamagnetism. The upper field, H_{c2} is the value at which superconductivity is destroyed. It can be calculated as [6]

$$H_{c2} = \frac{\Phi_o}{2\pi\xi^2}. \tag{1.15}$$

The phase diagram is given in Fig. 1.3. The scale on Fig. 1.3 is a few orders of magnitude larger than the scale on Fig. 1.2 (See Table 1.1). Both the upper and the lower critical fields can be related to the Ginsburg-Landau parameter given in Eqn. 1.12 and the thermodynamic critical field given by Eqn. 1.1 [8].

$$H_{c1} = \frac{1}{\sqrt{2}\kappa} H_c \ln\kappa \tag{1.16}$$

$$H_{c2} = \frac{\kappa}{\sqrt{2}} H_c \tag{1.17}$$

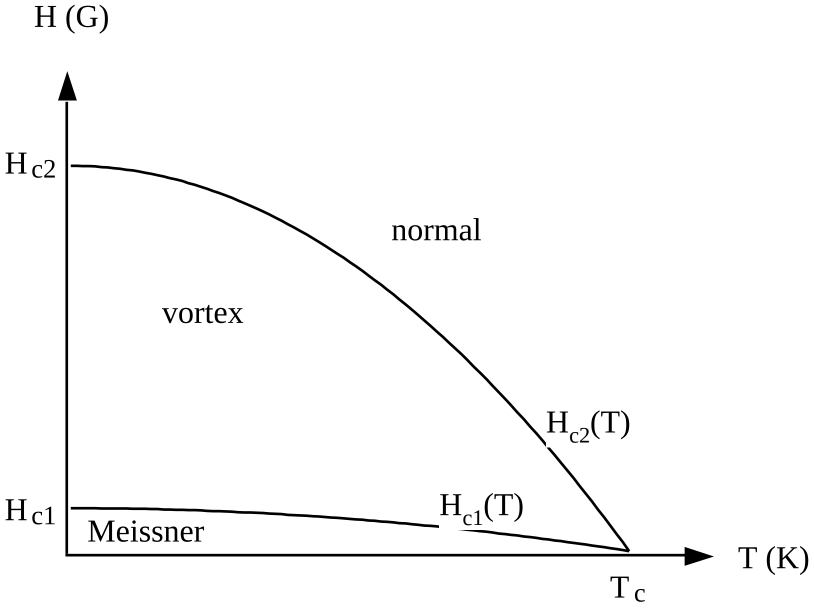

Figure 1.3: H-T phase diagram for a Type II superconductor.

The region in between the two fields is known as the vortex state. This is the region where flux lines may penetrate without destroying the superconductivity.

As Eqn. 1.17 makes clear, this region will be larger as κ is larger. Note that the vortex state is not a region of perfect diamagnetism.

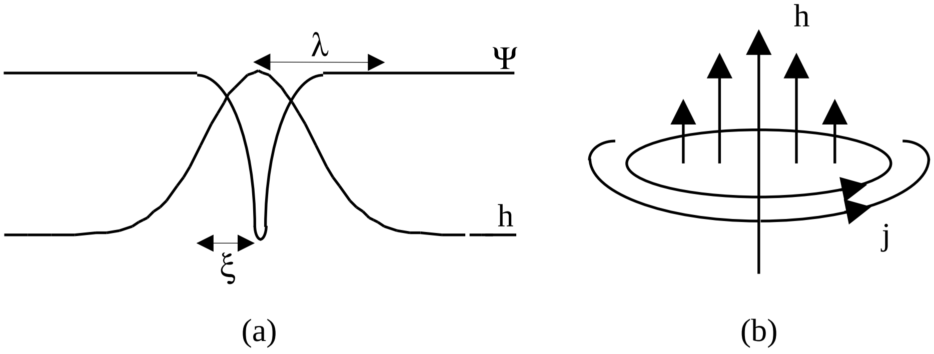

Figure 1.4: Structure of a vortex. a) The superconducting parameter goes to zero in the center of the vortex. b) The direction of supercurrent flow follows the right hand rule.

The structure of a vortex can be seen in Fig. 1.4. The vortex can be thought of as having a normal core of radius ξ and a field which falls off over a distance λ (Fig. 1.4a). The superconducting carriers flow around the flux line according to the right hand rule (Fig. 1.4b). This "whirlpool" motion is what gives rise to the name "vortex", in direct comparison to a hydrodynamic vortex.

There are two simple competing models for vortex structure, the Bardeen-Stephen (BS) model [9] and the Nozieres-Vinon (NV) model [11]. The BS model assumes a fully normal core surrounded by a finite transition region. Half the force felt by a vortex is experienced in this transition region. The NV model does not assume a transition region. Instead, there is a discontinuity in going from the normal core to the superconducting surroundings.

The number of vortices will increase with increasing field until their cores begin to overlap. This happens at the upper critical field, H_{c2}.

1.4 Motion of Vortices and the Anomalous Hall Effect

Vortices can form many states. There are vortex solids, liquids, and glasses. The most famous of these is the triangular Abrikosov lattice [12]. In the presence of a transport current, the vortices will experience a drive force which will make them move. Once in motion, there are other forces which come into play. In particular, the motion of a normal core of electrons introduces a viscous force, which introduces dissipation. Currently, the exact form of the equation of motion of a driven vortex is a matter of some controversy. We introduce a technique to measure forces directly, thus giving an estimate of their magnitude. This estimate can be used to evaluate differing theories of the equation of motion for a moving vortex.

Measurements of transport properties, in particular the Hall effect, have provided materials physicists with a convenient method for characterizing new materials. It was only natural that these measurements should be tried on the new, high-T_c materials. However, the Hall results were difficult to interpret. The sign of the Hall coefficient changed with temperature.

To see why this would be a problem, what follows is a review of the Hall effect in ordinary materials.

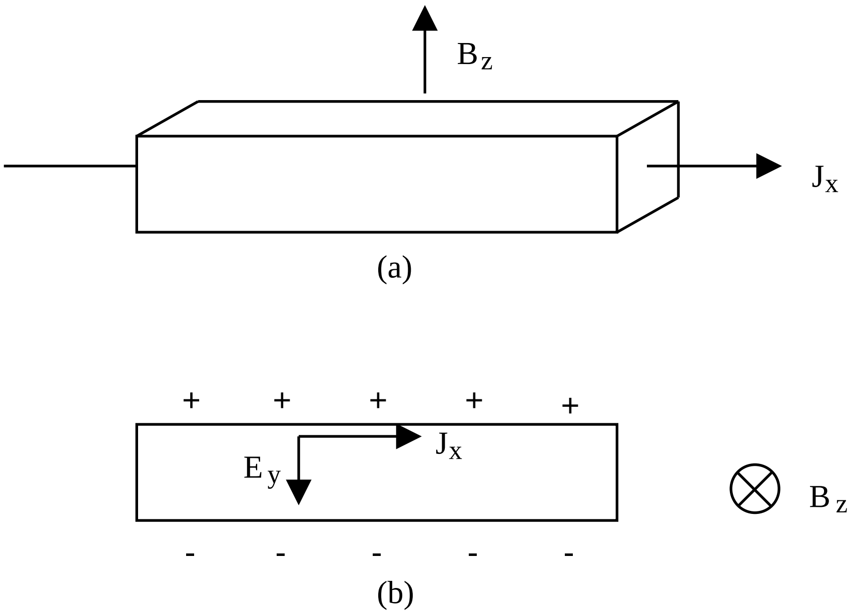

Figure 1.5: Standard geometry for measuring the Hall coefficient. a) Situation as t=0 when the fields are turned on. b) Steady state conditions.

Charged particles moving in a magnetic field will experince a Lorentz force

$$\vec{F} = q\vec{v} \times \vec{B}. \tag{1.18}$$

If the particles are constrained, for instance in a finite slab, there will be charge built up on one side of the slab. This situation is illustrated in Fig. 1.5 for the case of positive charge carriers. As the charged particles build up, an electric field will be generated. The electric field will continue to build until the force on the carriers balances the Lorentz force. In standard Hall geometry (as illustrated in Fig. 1.5), the transport current, applied magnetic field, and induced electric field are mutually perpendicular. The Hall coefficient is defined by

$$R_H = \frac{E_y}{J_x B_z} = -\frac{1}{ne}. \tag{1.19}$$

The Hall resistivity is defined by

$$\rho_{xy} = \frac{E_y}{J_x} \tag{1.20}$$

and is denoted ρ_{xy} to distinguish it from longitudinal resistivity, denoted ρ_{xx}. The Hall coefficient can be measured very easily by setting up a sample in the geometry illustrated in Fig. 1.5, sending a known current in the x-direction, applying a known field in the z-direction, and measuring the voltage drop in the y-direction. One can then find the sign and concentration of charge carriers. In the event that there are two types of carriers, for instance, in a semiconductor, Eqn. 1.19 can be generalized to

$$R_H = \frac{1}{e}\frac{p - nb^2}{(p + nb)^2} \tag{1.21}$$

where $b = \mu_e/\mu_h$ is the mobilty ratio [8].

Typical Hall measurements on copper-oxide superconductors show a strong temperature dependence [13]. This was hypothesized to be due to vortex motion which does not follow the transport current. Bardeen and Stephen [9] assert that there can be no interior stresses associated with supercurrent flow. They conclude that the Hall effect must come from a boundary – that is, vortices. In the hydrodynamic picture, the mean flow of the vortices is downstream along the direction of the transport current. The sign change in the Hall effect implies that vortices may move contrary to or at an angle to the transport current. This implies the presence of forces in addition to the drive force. The temperature dependent behavior implies different temperature regimes for the dominance of any given force. A correct description of vortex motion should explain the Hall anomaly.

The Hall effect continues to be used to study vortex motion [14, 15, 16], but it is an extremely indirect method.

1.5 The Form of the Equation of Motion

The exact form of the equation of motion of a moving vortex is the subject of some controversy and has been for over thirty years. Some argue that the controversy is a question of semantics [11, 17]. However, what remains is a severe lack of agreement on the part of theorists.

A general form of the equation of motion (in force per unit length) includes a massive term, a dissipative term, a pinning term, and a transverse term.

$$\vec{F}_{ext} = m_v \vec{a}_v + \eta \vec{v}_v + \vec{F}_T + \vec{F}_{pin} \tag{1.22}$$

The external force $\vec{F}_{ext}$ can contain a drive force, for instance, the Lorentz force.

This generic division of forces is a point of agreement for many authors. It is generally accepted that all the above terms – Lorentz, massive, pinning, viscous, and transverse – should be present, although some authors prefer to work in regimes where some of the terms may be neglected. What is a source of controversy is the grouping of these terms into an expression which is then labelled a force and given a name. Most of the controvesy is over the form of the transverse force, with the massive term generally ignored and the pinning and viscous terms at least accepted as existing. Presented here is a short discussion of the individual terms.

1.5.1 Massive Term

Vortex mass has electronic, electromagnetic, and strain field contributions. The electronic contribution is generally larger than the other two, but under certain circumstances the electromagnetic contribution can become quite large, e.g., a Josephson vortex in an individual junction.

A simple estimate of the electronic contribution to the vortex mass can be made using the local change in dispersion in the vortex core. The number of electrons experiencing this change can be found by multiplying the change in energy due to confinement in the vortex core by the density of states per spin at the Fermi level. The result is

$$m_v = \frac{2}{\pi^3} m_e k_F. \tag{1.23}$$

The massive term is very small and can generally be neglected.

1.5.2 Viscous Drag Term

When the drive force is larger than the pinning force (discussed below), the vortices will become unpinned and move. This is known as the "flux flow" regime. Their motion is limited by viscous drag, which gives rise to dissipation. Bardeen and Stephen [9] assert that for a moving vortex, relaxation processes which scatter electrons to the lattice will introduce a normal state component to the tranport current. This normal component gives rise to viscous drag and dissisipation. At $T = 0$, the normal component is large only near the core. Dissipation may also be approximately accounted for if the transport current flows directly through the normal core [10].

The viscous term is universally accepted as being of the form

$$\vec{F}_{visc} = -\eta \vec{v}. \tag{1.24}$$

where v is the velocity of the vortex, and η is the dissipation coefficient. The dissipation coefficient in the Bardeen-Stephen (BS) model [9] is

$$\eta = \frac{\Phi_o H_{c2}}{c^2 \rho_n} \tag{1.25}$$

where Φ_o is the flux quantum, H_{c2} is the upper critical field, ρ_n is the normal state resistivity, and c is the speed of light. The units of η are g/cm-s.

1.5.3 Pinning Term

In the presence of a drive current, vortex may get pinned on defects such as twin boundaries or oxygen vacancies, in the case of coppper-oxides. The mechanism is a defect-induced variation in the free energy which causes some locations to be more favorable than others. To be truly effective, the inhomogeneity must be on the order of the characteristic length scales of the material, ξ and λ. Defects which are smaller than this will cause scattering rather than pinning.

Pinning is a desirable phenomenon. We wish to have superconducting materials which can carry very high current with no dissipation. Transport current will flow around the core of a pinned vortex, eliminating the source of dissipation [9].

At sufficiently low temperature, all vortices will be pinned. At higher temperatures, some vortices will have sufficient thermal energy to overcome the pinning potential and hop from pinning site to pinning site. This phenomenom is known as "creep". Creep is usually a group phenomenom. Individual vortex motion is discouraged by the repulsive inter-vortex force. Vortices are expected to move in bundles when the drive force is large enough to overcome the pinning force. This bundle idea is supported by noise measurements in the flux-flow regime [18].

For fully pinned vortices, the pinning force takes the form of a restoring force

$$\vec{F}_{pin} = -k\vec{x}. \tag{1.26}$$

When the drive force becomes sufficiently strong or the temperature becomes sufficiently high, the vortices will completely depin and begin to move in response to the drive. The pinning force is proportional to $\vec{x}$, while the viscous force is proportional to $\dot{\vec{x}}$. This shift enables the detection of the pinning-viscous transition.

1.5.4 Transverse Forces

The exact form of the transverse force is the subject of some debate. In the case of a vortex at rest with respect to the lab frame, the Lorentz force takes the form

$$\vec{F}_L = \frac{\Phi_o}{c}\vec{j} \times \hat{n} = \rho_s \frac{\Phi_o}{c}\vec{v}_s \times \hat{n} \tag{1.27}$$

When the vortex begins to move, the force takes the more general form

$$\vec{F}_M = \rho_s \frac{\Phi_o}{c} (\vec{v}_s - \vec{v}_v) \times \hat{n} \tag{1.28}$$

This force is the Magnus force and can be derived from hydrodynamic considerations.

Ao and Thouless [23] give the vortex velocity contribution to the transverse force as

$$\vec{F}_T = \frac{\Phi_o}{c} \rho_s \vec{v}_{vortex} \times \hat{z}. \tag{1.29}$$

In a later paper, Thouless, Ao, and Niu [24] give the transverse force as

$$\vec{F}_T = \rho_s \kappa_s \times \vec{v}_{vortex} \tag{1.30}$$

Kopnin and Kravtsov [19, 20] and Kopnin and Salomaa [21] give the transverse force as

$$\vec{F}_T = \frac{\Phi_o}{c} \rho_s \frac{\omega_o^2 \tau_r^2}{1 + \omega_o^2 \tau_r^2} \vec{v} \times \hat{n}. \tag{1.31}$$

The characteristic frequency ω_o is given by the level separation of the quasiparticle states bound to the vortex core. The characteristic time τ_r is the scattering relaxation time. Feigel'man [22] adds a term of the form

$$\delta \vec{F}_T = \frac{\Phi_o}{c} \delta \rho \vec{v} \times \hat{n} \tag{1.32}$$

Recent measurements support theories in which the transverse force is small [25].

1.6 Previous Experiments

In recent years, the vibrating superconductor (VSC) technique has become very popular for the study of vortex dynamics. Periodic tilting of a sample in a dc field is equivalent to making measurements on a stationary sample in an ac field. The sample experiences a field component of the dc field. The ac field experienced by a vibrating sample is very low due to the small oscillation amplitude. The VSC technique encompasses pendula [26], vibrating reeds [27, 28], and mechanical oscillators [25, 29, 30]. The frequency range available ranges from 10^{-5}-10^{1} Hz for subresonant excitation [26, 33], 10^{2}-10^{3} Hz for resonant pendula [31] to 10^{4} Hz for mechanical oscillators [25, 29, 30].

A subresonant torsional pendulum was developed to measure the energy loss per cycle, or internal friction, in a sample [32]. This technique is based on a technique for measuring anelastic properties of normal metals [33]. Excitation comes from a harmonic current through coils. Detection is via a laser reflected off a mirror to measure the deflection of the sample. When adapted for use with type II superconductors, the subresonant technique can measure anelastic properties of the flux line lattice [26]. Resonant techniques allow measurement only at one frequency. The subresonant torsional pendulum allows frequency-dependent measurements of internal friction in the sample. Changes in the internal friction can be related to dissipation peaks of stable flux-latices and flux creep of metastable flux-lattices.

A resonant pendulum in the form of a beam shaped sample suspended by fine wires [31] has also been shown effective at measuring dissipation. The drive is from a small alternating current which produces a Lorentz force. The motion of the sample in a magnetic field produces an induced voltage. This voltage is a measure of vibration amplitude. Experiments of this nature can be performed at only the resonant frequency, but temperature and field-dependent measurements are possible. Dissipation as a function of temperature indicates depinning transitions.

The vibrating reed can take the form of either a reed of superconducting material [34], or a reed of normal material with the superconducting sample attached to one end of the reed [27]. One end of the reed is clamped, and the other end is free to vibrate. The sample sees an ac field component which is perpendicular to the applied dc field [27]. The motion of the reed is driven and detected capacitively. AC susceptibility measurements are made on the sample. The results are interpreted as evidence for vortex dynamics such as melting [35] and depinning [27]. Reviews of the vibrating reed technique can be found in [36] and [37].

The vibrating reed technique has been adapted to measure forces on vortices in superconducting films directly [38]. The source of the drive is a vibrating magnet, and the pick-up is capacitive. They measure transverse forces. This experiment is the only one which is similar to the one described herein in that it is the only experiment which measures a force directly.

The flux dynamics reported in the above studies are very general, *e.g.*, the results may be dissipation peaks. A value of the dissipation coefficient for various high-T_c materials has not been reported.

High-Q, multimode, mechanical oscillators which are micromachined out of silicon were developed by Kleiman [39]. We have adopted this technique for our current study.

1.7 Estimate of Viscosity

The BS model provides an estimate of viscosity (Eqn. 1.25). This number is very easy to calculate. The value of Φ_o is given by Eqn. 1.13. For the characteristics of $Bi_2Sr_2CaCu_2O_8$, we turn to the literature. We estimate $H_{c2}(77\text{ K}) = 7.5\text{ T}$ based on data from [40]. Normal state resistivity is estimated from data in [41]: $\rho_n(77\text{ K}) = 20\ \mu\Omega\text{-cm}$. To convert from Gaussian to experimental units, use 1 G = 1 erg / cm^3 and $1\ \Omega = \frac{1}{9} \times 10^{-11}$ s/cm. The result is

$$\eta = 8 \times 10^{-7} \frac{\text{g}}{\text{cm-s}}. \tag{1.33}$$

Chapter 2

Experimental Technique

The basic idea is to exploit the properties of mechanical oscillators to use them as pick-up devices in small force detection experiments. A high-Q (low damping) multimode oscillator is used. Attaching the sample to the head of the oscillator couples it directly to the oscillator. Forces which act on the sample are then transmitted to the oscillator. Direct measurement of the motion of the oscillator makes possible a direct measurement of the force.

2.1 Oscillating Systems

An oscillating system can be characterized by two quantities, the resonant frequency, f_o, and the quality, or Q, factor. The Q factor is expressed as

$$Q = 2\pi \frac{\langle E \rangle_{per\ cycle}}{E_{dissipated\ per\ cycle}} \tag{2.1}$$

and is a measure of the dissipation of the system.

We can write down Newton's second law in one dimension for a damped driven oscillator:

$$M\ddot{x}(t) + M\omega_o^2 x(t) + M\Gamma\dot{x}(t) = F_o cos(\omega t). \tag{2.2}$$

This has steady state solutions

$$x_{ss} = A_{ab}\sin(\omega t) + A_{el}\cos(\omega t) \tag{2.3}$$

where

$$\begin{aligned} A_{ab} &= \frac{F_o}{M}\frac{\Gamma\omega}{(\omega_o^2-\omega^2)^2+\Gamma^2\omega^2} \\ A_{el} &= \frac{F_o}{M}\frac{\omega_o^2-\omega^2}{(\omega_o^2-\omega^2)^2+\Gamma^2\omega^2} \end{aligned} \tag{2.4}$$

These amplitudes are graphed for an arbitrary system in Fig. 2.1.

The two amplitudes represent the in-phase component (A_{el}) and the 90° out-of-phase component (A_{ab}) where in- and out-of-phase refer to the driver.

Both Q and f_o are inherent to the system, and depend on the acting forces, *i.e.*, restoring or driving forces. Both these quantities can be measured from the absorptive amplitude. An alternate definition of Q is

$$Q = \frac{f_o}{\Delta f_{FWHM}} \tag{2.5}$$

where Δf_{FWHM} is the full width at half the maximum of A_{ab} (see Fig. 2.1).

A measurement of the amplitudes will then give information on the forces acting on the system.

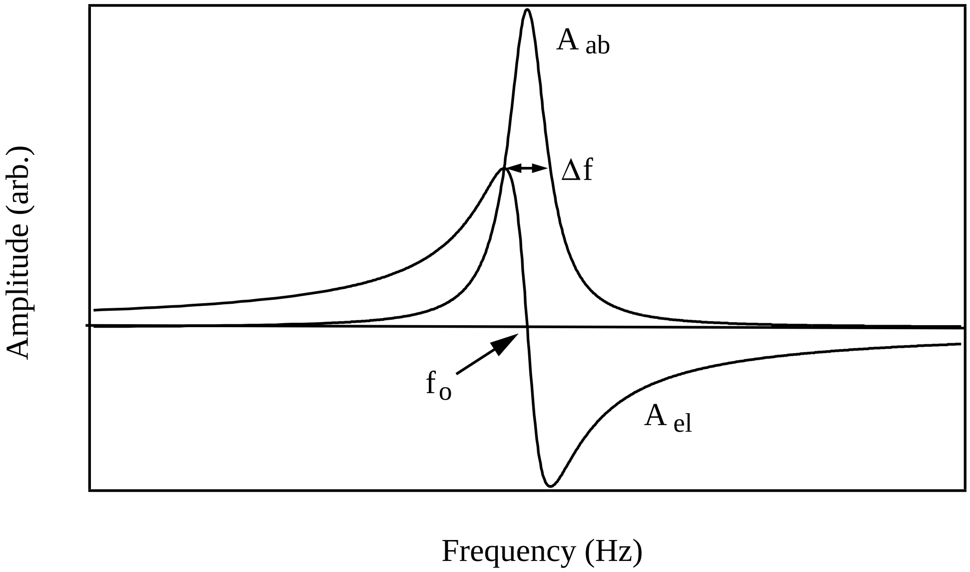

Figure 2.1: Solutions to Eqns. 2.4 for an arbitrary system.

2.2 Minimum Force

In reality, the equation of motion should include a thermal term to account for thermal fluctutations. This thermal noise sets a lower limit on the size of the force which the oscillator can detect. The minimum detectable force for a cantilever is [42]

$$F_{min} = \sqrt{\frac{4k_B k_s T \Delta\nu}{Q\omega_o}} \tag{2.6}$$

where k_s is the spring constant, k_B is the Boltzman constant, T is the temperature, $\Delta\nu$ is the bandwidth (determined by the time constant of the lock-in amplifier).

The minimum detectable force can be minimized by raising the Q, lowering the temperature, or lowering the spring constant. Using single crystal materials to make the oscillator reduces internal disspation from defects, raising the Q. Use of a double torsional design (see Fig. 2.2) isolates the clamped base (high dissipation) from the mobile head (lower dissipation), which also raises the Q. The spring constant is related to the geometry of the oscillator, and also the mode of oscillation. Scaling down the size of the oscillator can lower the spring constant.

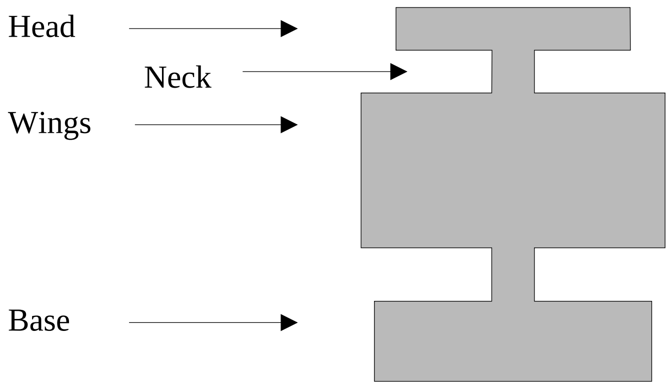

Figure 2.2: Design of a double torsional oscillator. The head and wings are free to move. The base is clamped.

2.3 Modes

The double torsional design has two masses – the head and the wings (see Fig. 2.2). This results in two normal modes for each translational and rotational degree of freedom, resulting in twelve modes total. We commonly examine only four modes. Recent calculations identify more modes [44]. The common modes are illustrated in Fig. 2.3. Fig. 2.3a shows the torsional modes, and Fig. 2.3b shows the cantilever modes. The torsional modes are so named because the motion twists about the axis of the necks. The cantilever modes bend at the necks. Both torsional and cantilever modes have an upper mode where the motion of the head and wings is in the opposite sense, and a lower mode where the motion of the head and wings is in the same sense. Approximate typical frequencies of these modes for the oscillators manufactured by the Markert group (see Sec. 4.2 for full manufacturing details) are, from lowest to highest: lower cantilever, 1800-2000 Hz, lower torsional, 2000-2200 Hz, upper cantilever, 6700-7400 Hz, upper torsional, 11,000-13,000 Hz. There is an asymmetry between the amplitudes of the torsional and cantilever modes which is geometrical in nature. In the cantilever mode, the drive and pick up wings move in phase – they are always the same distance from the electrodes. In the torsional mode, the drive and pick up wings move out of phase- when one is furthest away, the other is closest. The result is that characteristic sweeps of cantilever and torsional modes will be 180° out of phase with each other. The upper modes, in which head and wings move in the opposite sense, have much higher Q's. This is because the head is decoupled from the lossy base in the upper modes.

2.4 Modeling the System

The motion of the various modes has been modelled in some detail elsewhere [45]. Presented here is an outline of the model, along with the major results. The focus of this section is on the cantilever modes, as the bulk of the experiments were done using this mode.

A simple model of a double torsional mode is two rigid bars connected to

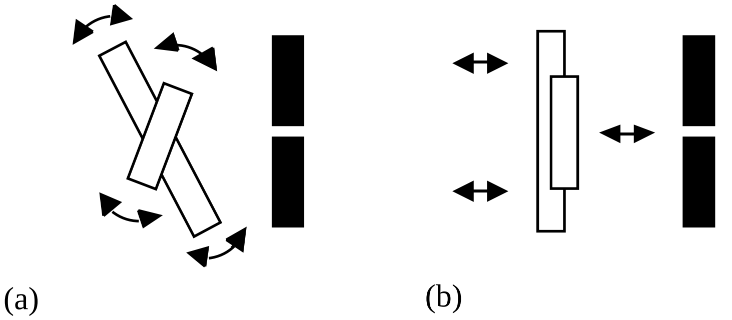

Figure 2.3: Modes of a double torsional oscillator. The open boxes represent the head and wings of the oscillator. The filled boxes represent the electrodes. a) Torsional modes. b) Cantilever modes. In the upper modes, the head and wings move in the same sense. In the lower modes, the head and wings move in the opposite sense.

each other and to an infinitely massive base via a thin wire as in Fig. 2.4. The torsional mode is a twisting mode, so it can be examined in terms of the angles with respect to the base θ_1 and θ_2 made by the head and base, and the torques τ_1 and τ_2 on the head and base.

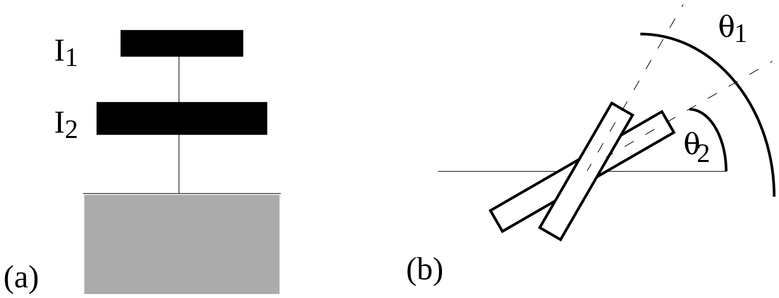

Figure 2.4: A simple model of the torsional modes. a) A physical model of the system. b) Top view showing twisting motion. The angular deflection is exaggerated for the sake of clarity.

The equations of motion of the system in the absence of external torques are:

$$\begin{aligned}\tau_1 &= -\kappa(\theta_1-\theta_2) = I_1\frac{d^2\theta_1}{dt^2} && (2.7)\\ \tau_2 &= -\kappa\theta_2 && (2.8)\\ \tau_2-\tau_1 &= I_2\frac{d^2\theta_2}{dt^2} && (2.9)\end{aligned}$$

where I_1 and I_2 are the moments of inertia of the head and wings, and κ is the torsional spring constant of both bars of the oscillator, assumed identical. The torsional spring constant, κ, can be expressed in terms of material parameters [46]:

$$\kappa = \frac{Gwt^3}{h}\frac{1}{3}\left(1-\frac{192}{n^5}\frac{t}{w}\sum_{n=0}^{\infty}\frac{1}{(2n+1)}\tanh\left((2n+1)\pi\frac{w}{t}\right)\right) \qquad (2.10)$$

where G is the sheer modulus of the material, and h, t, and w are the height, thickness, and width, respectively, of the oscillator. This expression can be approximated safely to within 4% as [47]

$$\kappa = \frac{Gwt^3}{h}\left(\frac{1}{3}-0.209\frac{t}{w}\left(1-\frac{1}{12}\left(\frac{w}{t}\right)^4\right)\right) \qquad (2.11)$$

If we assume a sinusiodal dependence for θ_1 and θ_2 of the form $\theta = \theta_o \mathrm{e}^{-i\omega t}$, we can substitute these solutions into Eqns. 2.7 and solve to find resonant frequencies of the torsional modes:

$$\omega^2 = \frac{\kappa}{2I_1I_2}\left(2I_1+I_2\pm\sqrt{4I_1^2+I_2^2}\right) \qquad (2.12)$$

The positive root is the antisymmetric mode and the negative root is the symmetric mode. The moments of inertia are easily calculated. Real oscillators do not have easily measured dimensions due to the nature of the production process (see Fig. 4.3 and Sec. 4.2.4). The dimensions of one particular oscillator were measured to be [45] 8.28 × 2.65 × .53 mm^3 for the head and 7.24 × 8.24 × .53 mm^3 for the wing. The density of silicon is 2.328 $\mathrm{g/cm}^3$ [49]. These values used in Eqn. 2.12 give the resonant frequencies of the upper and lower torsional modes, and the ratio of the resonant frequency of the upper mode to the resonant frequency of the lower mode.

$$\omega_{ut} = 14 \text{ kHz} \tag{2.13}$$

$$\omega_{lt} = 2.5 \text{ kHz} \tag{2.14}$$

$$\frac{\omega_{ut}}{\omega_{lt}} = 5.5. \tag{2.15}$$

The presence of additional forces on the oscillator will introduce additional terms in the equations of motion. We are interested in the presence of a viscous force on the head of the oscillator, the source of which is a moving flux line. The equations motion take on the form

$$-\kappa(\theta_1 - \theta_2) - \eta r^2 \frac{d\theta_1}{dt} = I_1 \frac{d^2\theta_1}{dt^2} \tag{2.16}$$

$$-\kappa(2\theta_2 - \theta_1) = I_2 \frac{d^2\theta_2}{dt^2} \tag{2.17}$$

where η is the viscosity, A is the amplitude of motion of the flux line, r is the distance from the axis of rotation to the point where the viscous force acts, and the other variables are as above. We solve this system so that the results may be used during analysis.

Assume a sinusiodal dependance as before, the equations become

$$\begin{aligned} -\kappa(\theta_1 - \theta_2) + i\omega\eta r^2\theta_1 &= -I_1\omega^2\theta_1 & (2.18) \\ 2\kappa\theta_2 - \kappa\theta_1 &= -I_2\omega^2\theta_2. & (2.19) \end{aligned}$$

These equation can be rewritten in matrix form:

$$\begin{pmatrix} \frac{I_1\omega^2}{\kappa} - 1 + \frac{i\omega\eta r^2}{\kappa} & 1 \\ 1 & \frac{I_2\omega^2}{\kappa} - 2 \end{pmatrix} \begin{pmatrix} \theta_1 \\ \theta_2 \end{pmatrix} = 0 \qquad (2.20)$$

To have non-trivial solution, the determinant must vanish:

$$\left(\frac{I_1\omega_v^2}{\kappa} - 1 + \frac{i\omega_v\eta r^2}{\kappa}\right)\left(\frac{I_2\omega_v^2}{\kappa} - 2\right) - 1 = 0 \qquad (2.21)$$

where the notation ω_v reminds us that we are interested in the resonant frequency in the presence of a viscous force. When written out fully, the determinate is

$$\frac{I_1I_2}{\kappa^2}\omega_v^4 + i\frac{\eta r^2 I_2}{\kappa^2}\omega_v^3 - \frac{I_2 + 2I_1}{\kappa}\omega_v^2 + i\frac{2\eta r^2}{\kappa}\omega_v + 1 = 0. \qquad (2.22)$$

The anticipated frequency shift is very small. We make this equation more easily solvable by making the selective approximation of $\omega_v \approx \omega_o$.

$$\frac{I_1I_2}{\kappa^2}\omega_v^4 + \left(i\frac{\eta r^2 I_2\omega_o}{\kappa^2} - \frac{I_2 + 2I_1}{\kappa}\right)\omega_v^2 + \left(i\frac{2\eta r^2\omega_o}{\kappa} + 1\right) = 0. \qquad (2.23)$$

This approximation transforms the determinate from a fourth order equation in ω_v to a second order equation in ω_v^2. The real part is

$$\omega_v^2 = \frac{\kappa}{2I_1I_2}\left[I_2 + 2I_1 \pm \sqrt{I_2^2+4I_1^2}\left(1 - \frac{1}{2}\frac{(\eta\omega_o r^2 I_2)^2}{\kappa^2(I_2^2+4I_1^2)})\right)\right] \tag{2.24}$$

Using the plus sign for the upper torsional mode, we find the frequency shift to be

$$\omega_v^2 - \omega_o^2 = -\frac{1}{4\kappa I_1 I_2}\left[\frac{(\eta\omega_o r^2 I_2)^2}{\sqrt{I_2^2+4I_1^2}}\right]. \tag{2.25}$$

This indicates that the frequency will decrease in the presence of a viscous force on the head.

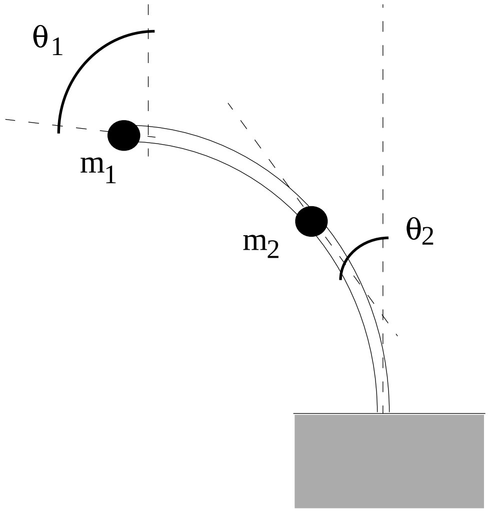

Figure 2.5: A simple model of the cantilever modes. The deflection from the vertical is exaggerated for the sake of clarity.

A simple model of a double cantilever mode is two point masses m_1 and m_2 at the head and wings connected to each other and to an infintely massive base via flexible bars of length l, as shown in Fig. 2.5. The vertical deflection in this figure is exaggerated for the sake of clarity. In reality, the deflection is small enough that the y coordinates of the two masses can be considered constant. Since the cantilever mode is a flexing mode, postions of the two masses is best expressed in terms of angles. The position of the wings, (x_2, y_2) should be expressed in terms of the angle the lower bar makes at the base, and the angle the lower bar makes at the wings, θ_2. The position of the head, (x_1, y_1), should be expressed in terms of the angle the upper bar makes at the wings, which is θ_2, and the angle the upper bar makes at the head, θ_1. The equation of motion for the system will be

$$\begin{aligned} m_1\left(\frac{\ddot{\theta}_1}{2}+\ddot{\theta}_2\right)l + k(\theta_1-\theta_2)l &= F_1\exp(i\omega t) && (2.26)\\ m_2\frac{\ddot{\theta}_2}{2} + k(2\theta_2-\theta_1)l &= F_2\exp(i\omega t) && (2.27)\end{aligned}$$

Here k is the flexing spring constant, related to the torsional spring constant κ by

$$k = \frac{\kappa}{l^2} \tag{2.28}$$

where l is the lateral distance along the oscillator to the point where the force acts. The force in our case is the capacitive drive force on the wing.

The resonant frequencies of the cantilever modes satisfy

$$\omega^2 = \frac{k}{m_1}\left(1+4\frac{m_1}{m_2} \pm \sqrt{1+4\left(\frac{m_1}{m_2}\right)+16\left(\frac{m_1}{m_2}\right)^2}\right) \tag{2.29}$$

The positive and negative roots are the upper and lower modes. For the oscillator mentioned above, this gives

$$\begin{aligned} \omega_{uc} &= 5.8 \text{ kHz} && (2.30)\\ \omega_{lc} &= 1.5 \text{ kHz} && (2.31)\\ \frac{\omega_{uc}}{\omega_{lc}} &= 3.8. && (2.32) \end{aligned}$$

In the presence of a viscous force on the head of the oscillator, the equations of motion take the form

$$\begin{aligned} m_1\left(\frac{\ddot{\theta}_1}{2}+\ddot{\theta}_2\right)+k(\theta_1-\theta_2)l+\eta\left(\frac{\ddot{\theta}_1}{2}+\ddot{\theta}_2\right) &= F_1\exp{(i\omega t)} && (2.33)\\ m_2\frac{\ddot{\theta}_2}{2}+k(2\theta_2-\theta_1)l &= F_2\exp{(i\omega t)} && (2.34) \end{aligned}$$

This system may be solved as for the torsional modes. However, as will be seen later, the frequency shift involved is practically unresolvable. For this reason, we do not use it in calculations.

The experiment involves driving the oscillator by both the head (viscous sweep) and the wing (capacitive sweep). In order to compare results with wing drive to results with head drive, we wish to know the difference in response between wing drive and head drive for the same driving force. For the case of head drive, $F_1 = F_o\exp{(i\omega t)}, F_2 = 0$. For the case of wing drive, $F_1 = 0, F_2 = F_o\exp{(i\omega t)}$. Using these in the equation of motion, we find

$$\frac{\theta_2(\text{wing drive})}{\theta_2(\text{head drive})} = 1-\frac{m_1\omega^2}{2k} = -0.56 \qquad (2.35)$$

where the result given is for the upper cantilever mode. The negative sign implies that the motion of the wings (θ_2) during head drive is opposite to the motion of the wings during wing drive for equal applied forces.

Chapter 3

Experimental Set-up

3.1 Overview

The probe used to carry out the experiments has been descibed in great detail elsewhere [45]. In brief, a high-Q, double torsional oscillator is used as a pickup device. A superconducting crystal sits on the head of the oscillator. An electromagnet aligned around the crystal provides the vortices. A tube piezo drives the magnet, and hence the vortices. What follows is a short description of the aforementioned parts, with the exception of the oscillators. The oscillators are described in detail in Chapters 2 (theory) and 4 (fabrication).

The inside of the probe is shown in Fig. 3.1.

3.2 Piezoelectric Tube

A piezoelectric tube drives the magnet. This piezo drive is what provides the drive force in the equation of motion. The piezo tube is manufactured by Staveley Sensors Inc. It is 1 in high by 0.375 in OD, with wall thickness .020 in. It is OD positive polarized. The inner wall is a single electrode, and the outer wall is divided into four quadrants. This four quadrant division makes possible drive in

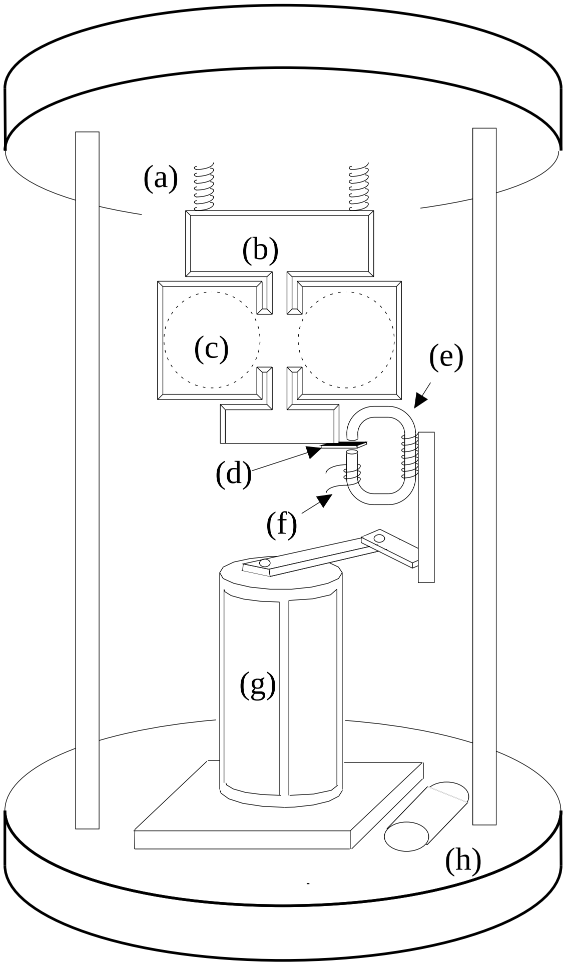

Figure 3.1: The inside of the probe. a) Isolation springs b) oscillator c) electrodes d) crystal e) electromagnet f) pickup coil g) piezo tube h) thermometer

two orthogonal directions, enabling the experimenter to examine separately forces parallel and perpendicular to the direction of motion.

The piezo also has resonances. In particular, it has very broad resonances in the 10-12 kHz range, making data taking in this area unfeasible.

The piezo was measured in real time at room temperature using an interferometric technique [45]. The results were extrapolated to liquid nitrogen temperature. The tube is estimated to have a 19 nm response to a 15 V drive. This is extrapolated to 13 nm for 10 V drive.

3.3 Electromagnet

The magnet which provides the vortices is made of a single coil of 200 turns of 38 AWG copper wire wound around an annealed iron core. Iron was chosen because it produced the largest emf of the materials tested [45]. The core diameter is .020 in. A pick-up coil around the core enables a measurement of the flux. Typical magnet currents are 120 mA. This produces a field of .158 T, and 1.54x10^7 vortices.

3.4 Electrodes

Electrodes are placed close to the oscillator wings to form a capacitor with each wing. A trapped charge is placed on the face of the oscillator by biasing at high voltage, V_{bias}, typically 250 V. Knowledge of the gap distance, d_{gap}, is essential. The gap is measured by inserting one of a variety of wires of differing diameters into the gap, finding one that fits, and measuring the diameter of the best fit wire.

3.4.1 Drive

The oscillator is driven by application of a sinusiodal voltage of amplitude V_{drive} to the drive electrode. The drive voltage used depended on operating conditions. Driving the oscillator too hard is undesirable. A large drive results in a large response, and silicon has a finite ability to flex. A few oscillators went bad after being in use for prolonged periods. This may have been because they were driven too hard and formed micro-cracks. Drive voltages of 10 V at room temperature and 1 V at liquid nitrogen temperature keep the response to about 10 μV.

The force on the oscillator wing at the resonant frequency has amplitude

$$F = \frac{C_{gap} V_{bias} V_{drive}}{d_{gap}}. \tag{3.1}$$

The area of the electrodes is 4×10^{-5} m^2, so the capacitance of the gap can be calculated from:

$$C_{gap} = \frac{3.5 \times 10^{-18} \text{ F-m}}{d_{gap}}. \tag{3.2}$$

Typical motion of the oscillator wing due to this force has been measured to be 21 nm [48].

3.4.2 Pickup

A second electrode on the other wing on the oscillator provides capacitive pickup. The pick-up signal is directly proportional to the driving force, regardless of the nature of the drive.

The equation of motion for a capacitively driven system is

$$\frac{C_{gap} V_{bias} V_{drive}}{d_{gap}} e^{-i\omega t} - \Gamma(xe^{-i\omega t})' - k_s(xe^{-i\omega t}) = m(xe^{-i\omega t})'' \tag{3.3}$$

The complex solution to this is

$$x = \frac{F}{m} \frac{[(\omega_o^2 - \omega^2) - i\frac{\gamma}{m}\omega]}{[(\omega_o^2 - \omega^2)^2 + (\frac{\gamma}{m}\omega])^2} \tag{3.4}$$

where

$$F = \frac{C_{gap} V_{bias} V_{drive}}{d_{gap}} \tag{3.5}$$

At the resonance frequency of the ideal oscillator, the forced oscillator has real (absorptive) part

$$A_{ab} = \frac{FQ}{m\omega_o^2} = \frac{FQ}{k} \tag{3.6}$$

Here A_{ab} is the magnitude of the resonance signal from the lock-in, F can be calculated from Eqn. 3.5, and Q can be calculated from Eqn. 2.5. k in this case includes both the spring constant, and a conversion factor in $\frac{\mathrm{N}}{\mu\mathrm{V}}$.

The proportionality factor k is used to convert the viscous signal peak to a force also using Eqn. 3.6:

$$F_{visc.} = \frac{A_{ab} k}{Q} = \eta v_{vortex} \tag{3.7}$$

3.5 Sample

A Japanese group [1] provided high quality BSCCO 2212 samples. These crystals are very large, single cystal without twin boundaries. The superconducting transition was measured using a Quantum Design SQUID Magnetometer. After one crystal went bad and stopped giving a signal, the crytals were characterized periodically to ensure that they were still superconducting. An example is in Fig.

---

[1] Y. Ando at CRIEPI, Tokyo, Japan

3.2. Many references can be found for the theory of SQUID measurement. To start, Tinkham's book includes a chapter on the subject [5].

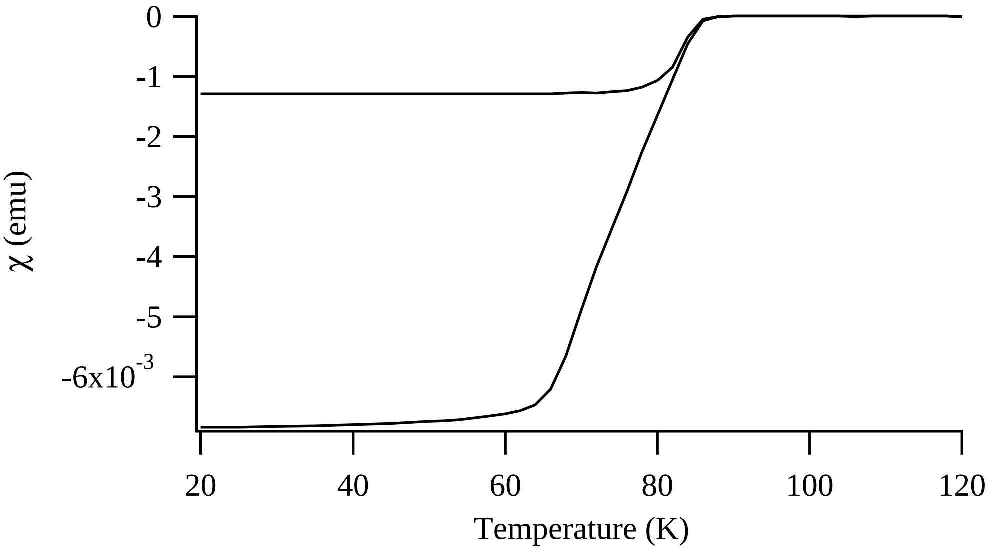

Figure 3.2: SQUID magnetometer characterization of the BSCCO crystal used in this work. Applied field is 10 G.

3.6 Dewar

Cooling and temperature control are provided by a Janis Research Co., Inc., dewar. This dewar has (in order from the center outward) a sample space, an inner helium jacket, an outer nitrogen jacket, and a vacuum jacket in between all. The system has temperature control capabilities between 1.5 K and 300 K. The control is provided by flowing helium vapor through a needle valve to the sample space. The helium exits the resevoir through the needle valve and enters a vaporizer. Once in the vaporizer, the LHe evaporates and warms to the desired temperature. There is a thermometer contained in the dewar as well as one on the probe. Full details of the dewar's construction and operation can be found in the operating instructions.

Data taken at 77 K are sometimes taken in a bucket dewar rather than the Janis system. Measurements above 77 K are taken in the Janis dewar with nitrogen in both the helium and nitrogen resevoirs.

Chapter 4

Silicon Processing

This chapter shall serve not just as an explanation of the process used to produce the oscillators in this study, but also as a guide for future fabricators.

4.1 Mask Fabrication

Oscillators were originally etched out of 3-inch wafers [45]. A new mask had to made to accommodate the larger surface area of the 4-inch wafers, and to increase yield.

4.1.1 Mask Design

A 10X enlarged positive image of the desired design was produced using PowerDraw. Design considerations for the mask are: alignment features for alignment to the wafer flat, sufficient space between structures, and correct spacing between the structures and the supporting wafer. As the etch proceeds along the <111> planes, it is essential that the pattern line up with these planes as well. A series of horizontal lines that can be aligned with the wafer flat ensure alignment of the oscillator features with the <111> planes. Ultimately, the wafers will be

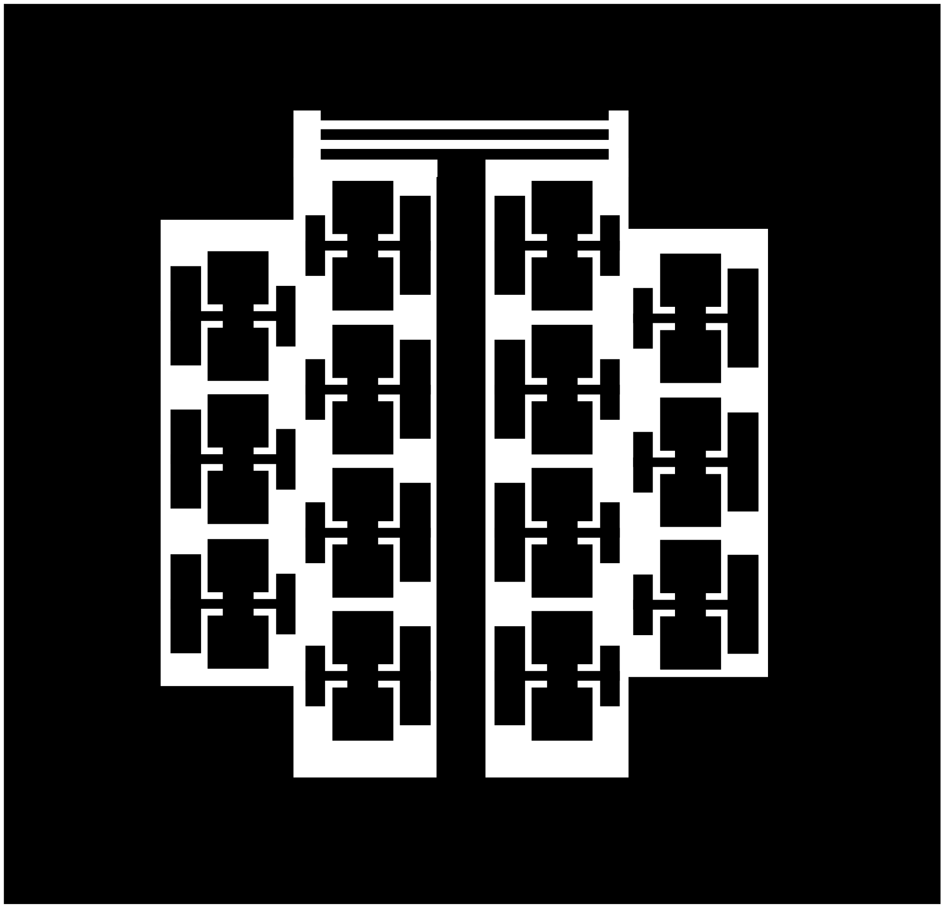

Figure 4.1: The mask pattern used to produce the oscillators. The lines at the top are to aid in alignment of the mask to the wafer flat.

immersed in a KOH bath (see Sec. 4.2.4). It is best for the oscillators to remain attached to the surrounding wafer during this step. If they fall, there is the possibility for breakage. Thus the distance between the oscillator and the surrounding wafer is calculated such that the oscillator will remain attached until the moment that the etch is complete. The inter-oscillator distance must be greater than the oscillator-substrate distance so that the oscillators will not be attached to one another. The final design is shown in Fig. 4.1.

An obvious, but important, consideration for mask design is that silicon wafers are round, and mask blanks are square. The seemingly wasted space in the corners of the design in Fig. 4.1 is unusable space.

A commercial vendor (Miller Blueprint, Austin, TX) shrank the image to 1X and produced a positive film. With the new mask, wafer yield increased from six oscillators per wafer to fourteen oscillators per wafer.

4.1.2 Glass Blanks

The blanks are 5 x 5 in. glass with a chrome coating from Nanofilm Inc. They were purchased with photoresist already spun on. This resist had been exposed to ambient lighting, and had to be washed off with considerable acetone.

4.1.3 Photolithography

The patterning is done in the class 100 cleanroom in the Microelectronics and Engineering Research Center Building (MERC) on the J. J. Pickle Research campus of the University of Texas. There are two lithography bays in the cleanroom, a silicon bay and a III-IV bay. All silicon patterning and silicon mask patterning must be done in the silicon bay.

Since the old photoresist had been ruined and cleaned off, new resist had to be spun on. First, primer is applied by an automated process (see App. B). This takes approximately twenty minutes to complete. The mask is now ready for photoresist.

The spinner has changeable chucks for different size wafers. The chuck for 6-inch wafers is best for 5-inch mask blanks. A smaller chuck will not provide sufficient support for the blank. Place the blank on the chuck metal-side up. The photoresist should be spun onto the metal coating. Use enough photoresist to cover most of the blank – this will be considerably more than is necessary for a wafer. Spin at 4000 rpm for 30 seconds. It is essential that the mask be centered. The spinner is designed for wafers, not mask blanks. The mask blanks are very heavy as compared to a silicon wafer, and misalignment of the blank from the center of the chuck may cause the blank to fall off, damaging both the blank and the spinner. After the photoresist has been spun on, the mask can then be prebaked for the litho step. Prebake on the hotplate at 90°C for a few minutes.

The patterning is done with the exposure system in the silicon bay. In addition to the mask blank and film, an additional blank with no resist or metal coating is necessary. The patterning tool has a mask holder (assuming you have a completed mask) and a wafer holder. Fasten the film, ink-side up, to the extra blank. Tape along the very edges is sufficient. Do not cover any part of the pattern with tape. This step is best done prior to entering the cleanroom, as there is no tape in the cleanroom. Place the blank with the film in the mask holder film-side up (the mask holder will turned upside down when it is inserted in the tool, resulting in the film facing downwards). Place the blank with photoresist on the wafer chuck resist-side up. The desired final configuration has the ink on the film in contact with the photoresist on the blank. Expose the mask (see App. B). Develop the photoresist and rinse with DI water. Postbake the mask for five minutes at 120°C.

The photoresist is now stabilized and the mask can be removed from the litho bay.

4.1.4 Metal Etch

The metal etch step takes place in the Markert lab. The chrome coating is removed with chromium mask etchant[1] followed by a rinse with sulfuric acid. The remaining photoresist is removed with acetone in the ultrasound cleaner. The mask is now complete.

4.2 Oscillator Fabrication

Oscillators are fabricated out of single crystal silicon wafers using standard integrated circuit processing techniques. The final product is of centimeter scale, so the processing is very simple. Only one mask layer is necessary, and the feature sizes are relatively large. The processing steps, in order, are: start with silicon wafers with 750 Å Low Pressure Chemical Vapor Deposition silicon nitride film predeposited. Pattern the nitride with photolithography, and use Reactive Ion Etch (RIE) to remove the exposed nitride. Etch the exposed silicon using potassium hydroxide (KOH) wet etch solution, and remove the remaining nitride with hydrofluoric acid (HF). Deposit metal on one side, attach lead wires, and mold an epoxy base. The litho and RIE are performed at MERC. Permission to use the facilities must be granted by the Facility Coordinator, currently William Fordyce. The remaining steps are performed in the Markert lab, with the exception of the metal deposition. The cryogenics staff performs this step. Details of each processing step follow. An overview of the process is shown in Fig. 4.2.

---

[1] Transene Co., Inc.

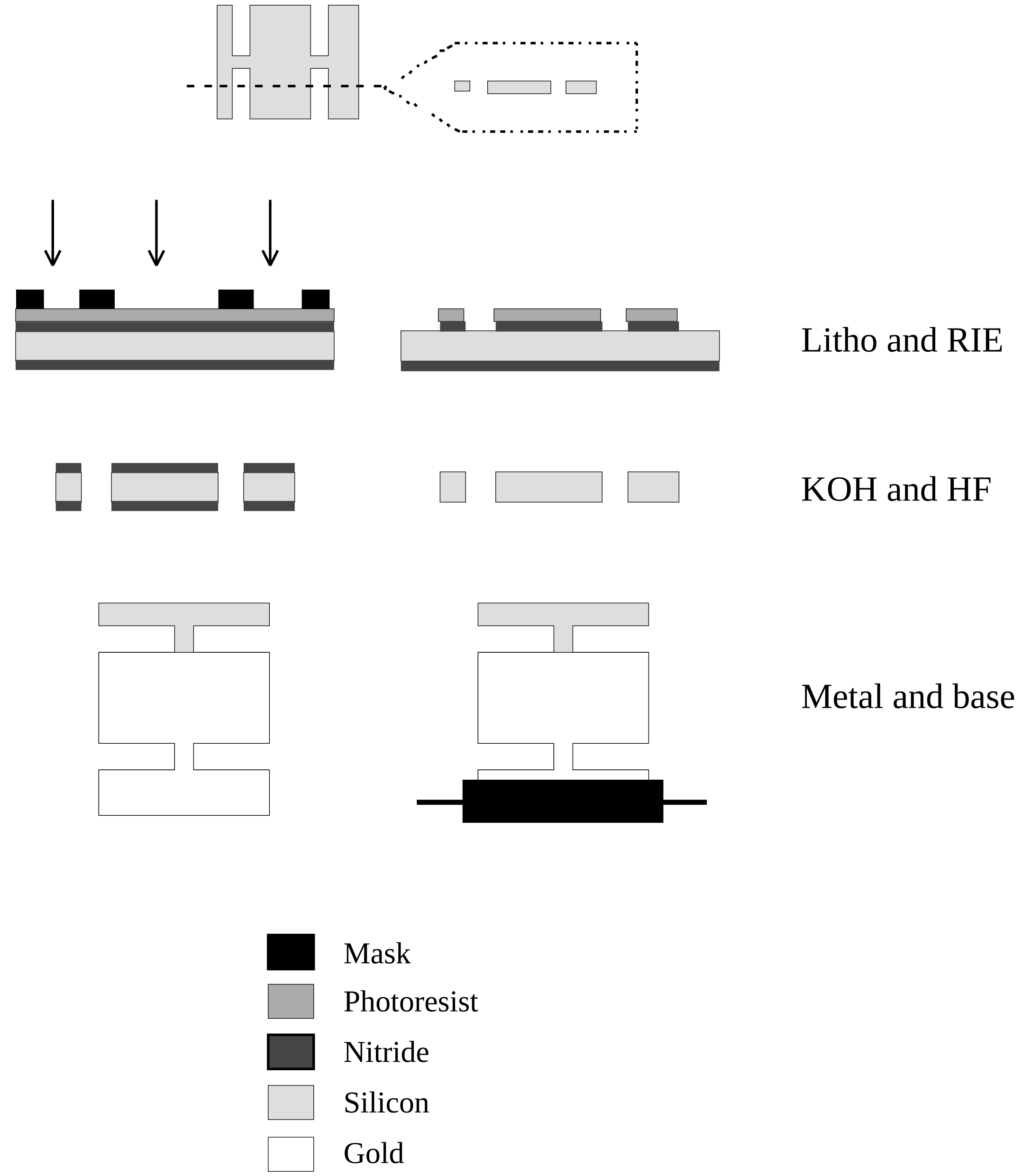

Figure 4.2: An overview of the oscillator fabrication process.

4.2.1 Wafers

The wafers are p-doped, 4-inch, (100), single-side polished purchased from Nova Electronic materials, Inc. The wafers are purchased with a LPCVD 750 Å Si_3N_4 film already grown on them. Alignment of the oscillator pattern with crystallographic planes is very important. A (100) wafer has <111> planes that cross it at right angles. These planes are parallel and perpendicular to the [110] flat (see Fig. 4.3). This is ideal for our oscillator pattern as it consists entirely of right angles. However, the <111> planes are not perpendicular to the (100) surface. Rather, they cross at an angle of 54.74°. This means that one face will always be smaller than the other face (see Fig. 4.3). The polished side of the wafer is designated as the "top", and it receives the patterning of the nitride. The polished face thus ends up as the smaller face.

4.2.2 Photolithography

The first step in photolithography is to spin on photoresist. The spinner has various size chucks – the correct size chuck for 4-inch wafers must be used. The photoresist at MERC is positive photoresist. That is, when the photoresist is exposed to UV light, the bonds are broken, and it can be washed away with developer. If a positive mask is used, a positive pattern is left on the resist. The resist and developer are AZ 5209-E and AZ 425 MIF, respectively, made and distributed by Clariant Corporation. First coat the wafers with primer (see App. B). This takes approximately twenty minutes to complete. When the wafers are cool enough to handle, place one on the spinner polished side up. Place 4-6

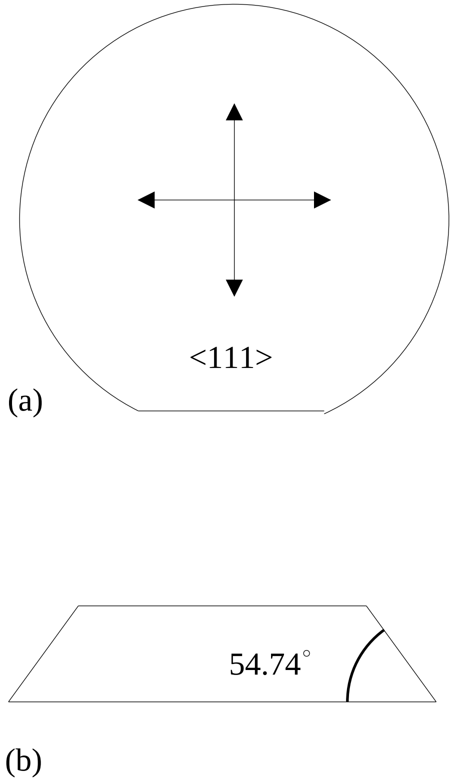

Figure 4.3: a) <111> planes with respect to the wafer face. b) Cross-section of the oscillator. The bevels are the <111> planes.

drops of photoresist in the center. More resist does not result in a thicker coating, it will only result in a worse smell. Spin at 4000 rpm for 30 seconds. To dry the photoresist, bake on the hot plate at 90°C for 1 min. This is referred to as the "pre-bake" because it takes place prior to exposure. The wafers are now ready to be patterned.

The patterning is done with the exposure system in the silicon bay (see App. B). The patterning tool has a mask holder and a wafer chuck. Place the mask in the mask holder metal-side up. Place the wafer on the wafer chuck resist-side up. The final configuration should have the metal on the mask in contact with the photoresist on the wafer. Use the alignment capabilities of the litho machine to align the mask with the wafer flat. This is essential to producing oscillators with straight sides. Once the mask is aligned, expose the wafer. Develop the photoresist and rinse with DI water. Post-bake the wafer at 120°C for one minute to dry the photoresist.

4.2.3 Reactive Ion Etch

Reactive Ion Etch (RIE) is a low pressure, plasma etch technique. It uses plasmas of freon and oxygen to bombard the surface with reactive ions. This technique is superior to others for the purposes of etching away the exposed nitride layer. Straight HF and boiling sulfuric acid will both etch nitride. However, the photoresist will not adhere in 50% HF solution, and boiling sulfuric is very slow. RIE is fast, and also has the benefit of being anisotropic [49].

RIE will etch photoresist at the same rate that it etches nitride. The spinning technique results in 3-4000 Å of photoresist, while there are only 750 Å of nitride. Thus there is no concern about overetch of the photoresist.

Details of the use of the RIE tool can be found in App. C.

4.2.4 KOH etch

A wet, KOH etch is used to etch the exposed silicon and release the structures from the wafer. The photoresist may or may not be removed prior to this step. The alcohol in the KOH solution attacks the photoresist and removes it completely within seconds. Etches both with and without photoresist have been performed, and no discernable difference in the final product has been noticed.

The wafer is mounted on a Teflon wafer holder. One wafer is processed at a time. Multiple wafers could be processed at one time. However, sometimes the etch results are poor, and it is best not to ruin more than one wafer at a time. With the new mask, yield per wafer increased to the point that multiple wafer etching is not necessary.

The etch solution most commonly used is 200 g KOH, 200 mL isopropyl alcohol, and 800 mL deionized water. KOH content has been increased to 250 g with no discernable effect. The etch solution is mixed in a plastic beaker which is then set inside a glass container in a double boiler arrangement. This maintains an isotropic temperature far better than placing the etch solution directly on the hotplate. A stir bar keeps the solution mixed to avoid compositional inhomogeneities. The etch takes place at approximately 80°C, and takes overnight. It is best to start the etch in the late afternoon. The temperature can then be monitored for stability prior to leaving it unattended overnight. The wafer will have etched through in approximately 24 hours. The etch rate depends exponentially on temperature, being faster at higher temperatures. The etch should be covered at all times to avoid excess evaporation. If significant evaporation occurs, a small amount of etch solution in the proper proportions may be mixed up and added to the bath.

Overetch is a significant problem with the KOH etch. The previous generations of oscillators were made from 3-inch wafers. These oscillators were etched in KOH until they fell free of the remaining wafer. The 4-inch wafers from which the current generation of oscillators is made are thicker than the 3-inch wafers. By the time the wafer has etched all the way through in the (100) plane, the (110) plane is also etching. This results in rounded corners. However, sometimes corner rounding occurs even before the etch has progressed significantly through the wafer. Etch bath temperatures between 60°C and 85°C have been tried, but the rounding seemed to occur at all temperatures. The round oscillators had Q's sufficiently high to pick up the desired signal, so the process conditions were let stand. A subsequent batch of wafers was processed under identical conditions, and square oscillators resulted.

It should be noted that the results of the KOH etch might depend intimately upon the prior history of the wafer. All the unprocessed wafers are assumed to be identical. All wafers processed at MERC at one time are assumed to be identical. Batches processed at MERC at the same time give the same results in the KOH etch. Batches processed at MERC at different times give different results in the KOH etch. Thus, the KOH etch may depend on factors involved with the RIE and the litho steps. For instance, since the photoresist is not removed before the KOH step, the age of the photoresist, either at spin on or after spin on, may influence the outcome of the KOH etch. Likewise, the RIE conditions may have an effect. At this time, there have not been sufficient batches of wafers processed for good quality control. Further, the conditions at MERC are completely out of Markert lab control. The result of a particular etch may never be traced back to its cause.

After being removed from the etch, the oscillators are placed in a plastic beaker of distilled water. Plastic beakers are always used because there is less chance that the oscillator will break upon contact with the beakers wall. After rinsing, the oscillators can either be blown dry with nitrogen or carefully dried with a Kimwipe. The oscillators are extremely fragile, and must be handled carefully. Blow-drying may result in the oscillator being blown out of the tweezers and broken. Wiping also has loss associated with it. Whichever method is used, the oscillators absolutely must be dried. Air-drying will result in water spots that can cause problems further down the road.

4.2.5 Edge trimming

The crystal that we study is mounted on the top edge of the oscillator. We wish the plane of the crystal to be absolutely perpendicular to the plane of the oscillator (see Fig. 3.1) . The crystallographic structure of the silicon wafers results in the oscillators' edges being non-perpendicular to the faces. To correct this, the top of the oscillator is sawed flat to provide a perpendicular edge to fasten the crystal to.

This “lobotomy” step could be performed at any point after the KOH etch which releases the oscillators from the wafer. However, this step has a very high oscillator loss rate, so it is best to perform it early. In particular, it is best to perform it before the HF etch. HF is extremely dangerous, and there is no sense in using it on an oscillator that may then break, wasting one's efforts.

The oscillator should be mounted with considerable paraffin wax on a carbon base, which is then mounted on an aluminum base. The bases and wax are heated on the hot plate. This should be done under the hood as the fumes from the hot paraffin are not particularly pleasant. It is very important that the oscillator lie very flat on the carbon base. If there are flecks of carbon or other material on the base, they must be removed. Slices in the carbon from previous cuts are not a problem. It is also very important that the entire oscillator be surrounded by wax. As long as there are no differential stresses on the oscillators, they are extremely robust. However, the slightest differential stress, for instance, from one side being more firmly attached by the wax than the other side, will lead to breakage.

Once the oscillators are attached and the wax has cooled and hardened, they may be brought to the diamond saw. The blade of the diamond saw must be aligned with the edge of the head of the oscillator. This alignment is easy to do by eye. Once the blade is aligned, the oscillator can be lobotomized. One has to be careful not to remove too much material, and keep in mind that the blade will remove a slice of material of finite width.

To remove the oscillators from the carbon/steel substrate, heat them on the hot plate until all the wax has melted, and slide them off. It is very important that the wax be completely melted. If part of the oscillator is still attached to the substrate, pulling it off will result in differential stresses and breakage.

The wax is removed from the oscillators by immersing them in boiling acetone. This is the only time that a glass beaker is used for the oscillators. A double boiler arrangement, similar to the KOH etch arrangement, would probably result in less breakage. The boiling acetone should definitely be kept under the hood as it produces poisonous fumes. The acetone should not boil too vigorously. Vigorous boiling produces bubbles which may break the oscillators. When the oscillators are clean, or mostly clean, they should be removed from the acetone and placed in distilled water. If there are stubborn spots of wax which do not come off in the acetone, they may be scrubbed off with an acetone soaked Q-tip. As long as the oscillator is perfectly flat, and not too much pressure is used, this will not lead to breakage. After all the oscillators are clean, they may be blown or wiped dry, as before.

Oscillators made from (110) wafers have flat heads already [39]. Cutting a flat edge on the head of the oscillators is a high loss procedure, and it is difficult to do correctly. Fabrication from (110) wafers is worth looking into.

4.2.6 Nitride Removal

The nitride layer on the oscillators is removed using 50% hydrofluoric acid (HF) solution. HF is extremely dangerous, and should not be used without proper safety precautions. These include full protective gear, use of a hood, access to calcium gluconate gel in case of exposure, access to either Epsom salts or calcium carbonate (lime) to pour on spills, and a large container of water to dilute the HF when the etch is complete. There should also be a clear path to the sink, and excess personnel should be discouraged from loitering in the immediate vicinity. HF absolutely should not be used unless there is another person in the lab to help handle possible emergencies.

After gearing up, the HF should be poured into the particular Teflon container that was made for this purpose. This container has a depression in the bottom that makes handling the oscillators easier. Only a few cc's of HF are necessary for this step. Using tweezers, place the oscillators in the HF. When they are fully etched, remove them with a tweezers, and place them in a large container of distilled water. The purpose of this water is to dilute any drops of HF that may cling to the oscillators.

It is easy to tell when the oscillators are fully etched. Bare silicon does not wet in water, while a nitride does. Just picking the oscillator up out of the HF solution will show whether the nitride is etched away or not. If it is etched, there will be at most one drop of HF adhering to the surface with a very high contact angle. If nitride remains, the entire surface will wet. Alternately, the etch may be timed to avoid excess handling of HF. The etch takes four minutes; five minutes is also okay. HF can roughen bare silicon, so excessive overetch should be avoided.

When all the oscillators are etched and in a distilled water bath, more distilled water should flow over the bath until the pH is sufficiently high. Nervous fabricators may use pH paper, but it is generally sufficient to allow an entire container of distilled water to flow over the bath. The excess HF should be poured into a plastic waste container for disposal by the UT Department of Environmental Health and Safety. Lime may be poured into the solution to titrate it, but this will be an extremely strong acid-base reaction and should be undertaken with extreme care.

The oscillators should be blown dry with nitrogen upon being removed from the distilled water. It is very important at this point that the oscillator surface be clean.

4.2.7 Metallization

The oscillators will be biased to high voltage. Silicon, even doped silicon, is not particularly conductive. A gold film is placed on the oscillators to enable them to hold a charge. The film must not be too thick because that will bring down the Q. Only the wings and base receive this film. The head and upper neck should be carefully wrapped up in Teflon tape to mask them off.

The cryogenics staff will evaporate 20 Å chromium and 100 Å gold onto the polished side of the oscillators.

4.2.8 Lead Wires

Lead wires are necessary to connect the oscillator electrically to the rest of the probe. The wire of choice is 22 AWG, solid, tinned copper wire (available from any electronics supply house). A fairly long piece is used because it forms the support during the base manufacture step. The wire is attached to the base of the oscillator with cryogenic silver epoxy (from Lakeshore) at two points. Two-point attachment provides a back up if one connection breaks. The silver epoxy is dried at 175°C for a few minutes to promote rapid shrinkage. The lead wire should be affixed fairly low on the base.

4.2.9 Epoxy Base

The oscillator is packaged with an epoxy base of Stycast 2850 MT (blue) resin and Catalyst 11 hardener mixed in 100:3 ratio by weight. A previous graduate student established this combination as having the least energy loss. The epoxy is poured into a Teflon mold, and the oscillator is inserted into the epoxy.

The resin must be mixed thoroughly before measuring. After mixing the resin with the catalyst, the epoxy must be pumped down to remove any mixed in air. This process takes about 5 minutes with a roughing pump and a bell jar.

Before the epoxy can be poured into the base mold, the mold must be prepared. The mold consists of three parts held together by screws. It should be completely disassembled prior to filling with epoxy. The bottom part of the mold, the part that the epoxy goes into, has a hole in the bottom to allow the finished product to be pushed out. This hole, and the openings for the lead wires, can be plugged up with vacuum grease. A thin coating of vacuum grease on the inside of the mold assists removal.

When the mold is greased up, pour the epoxy into it. Allow the epoxy time to settle, and screw the rest of the mold together. The pattern of screw holes in the various parts makes it obvious how the complete mold should be assembled (see Fig. 4.4). Of the two upright portions of the mold, one piece has two metal screws, and the other has one Teflon screw. These screws are for the purpose of keeping the oscillator upright. The Teflon screw is not necessary and may be removed. Place the oscillator in the mold so that the unpolished side faces the two metal screws. Push the oscillator far enough into the epoxy that the lead wire and silver epoxy are covered, but not so far that the bottom of the oscillator

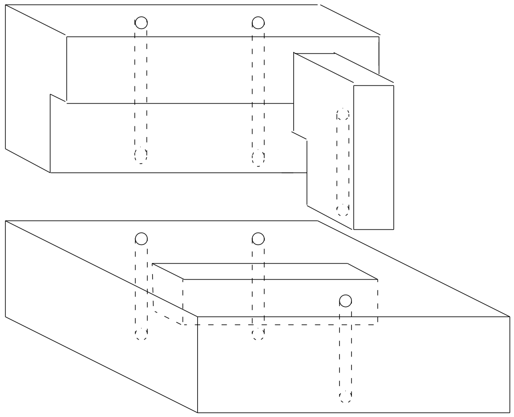

Figure 4.4: Assembly of mold for epoxy bases.

hits the bottom of the mold. A small portion of the base of the oscillator should protrude above the epoxy, but nothing should protrude on the other side of the epoxy base. The lead wire will support the oscillator within the epoxy mold. If there is epoxy leaking from any place, vacuum grease can be used to plug up the leak. The two metal screws are used to push the oscillator upright. On the other side, the polished side, a piece of folded paper can be used as a spring to hold the oscillator upright. The paper that is used must be stable at high temperature, as the epoxy needs to cure at high temperature. It is extremely undesirable to have the paper spring burst into flames during the cure. Weighing paper has the desired characteristics.

The Stycast epoxy needs to cure overnight at high temperature. The cure recipe is as follows: from room temperature, four hour ramp to 75°C, 12 hour hold at 75°C, 4 hour ramp to 120°C, 4 hour hold at 120°C, cool to room temperature. A previous graduate student established this heating recipe, except that he used

2 hour ramp times. The 4 hour ramp times are to avoid excessive thermal shock that could break the oscillator. The second soak time supposedly improves the epoxy. After cooling to room temperature. the oscillator may be removed from the oven and the mold, respectively. The epoxy base must be cleaned of all vacuum grease, taking care not to smear the oscillator itself. The oscillator is now ready to be mounted in the probe and tested.

Chapter 5

Corrosion resistant YBCO

At 77 K, flux lines in YBCO are completely pinned. This is partially due to the many twin boundaries in YBCO. YBCO is well known for having these boundaries, as well as for being extremely reactive to agents such as water, acids, CO_2, and CO [50]. In fact, $YBa_2Cu_3O_{7-\delta}$ shows the highest atmospheric corrosion reactivity of the technologically important cuprates with T_c above 77 K ($YBa_2Cu_3O_7$, $Tl_2Ba_2Ca_2Cu_3O_{10}$, $Bi_2Sr_2CaCu_2O_8$, and $HgBa_2Ca_2Cu_3O_9$) [50]. Explanations for this behavior have relied on copper valence arguments [51]. However, it has been shown that samples of $YBa_2Cu_3O_{7-\delta}$ with intermediate oxygen contents degrade less quickly than samples with high or low oxygen contents [52, 53]. This behavior is not explained satisfactorily along the lines of copper valence. Rather, extreme corrosion reactivity may be due to internal stresses caused by bond-length mismatches [54, 55]. Changes in oxygen content serve to influence the degree of bond-length mismatch [56]. The $YBa_2Cu_3O_{7-\delta}$ phase has an oxygen deficient, perovskite structure with a layer sequence $Cu(1)O_{1-\delta}$-BaO-$Cu(2)O_2$-Y-$Cu(2)O_2$-BaO-$Cu(1)O_{1-\delta}$ along the c-axis. This structure has poor bond-length matching between the Ba-O and the $Cu(2)O_2$ layers. Cation substitution strategies which lead to improved bond-length matching may be used to relieve this stress. The reduced stress may also lead to generally cleaner samples, resulting in reduced pinning. To investigate this possibility, we developed a technique to grow single-crystal samples of cation doped $YBa_2Cu_3O_{7-\delta}$ (TXYBCO) with decreased corrosion susceptibility. Increased resistance to corrosion will also allow for wet chemical processing in the fabrication of devices upon superconducting substrates. In this chapter, we present our method for growing TXYBCO crystals and examine their compositional, superconducting, and corrosion properties.

Previous studies have shown that substitutions on the Cu site normally decrease T_c dramatically [57]. The Y layer contains no oxygen, so substitutions at this site are expected to have only minor effects on the internal stresses [55]. Substitutions on the Ba site are thus expected to be the most successful. Substitutions of La^{3+} for Ba^{2+} relieve the bond strain, but cause a decrease in T_c due to disordering of the oxygen in the $Cu(1)O_x$ plane. A cosubstitution of Ca^{2+} for Y^{3+} has been shown [58] to maintain T_c above 80 K. Polycrystalline samples and films with the composition $Y_{1-y}Ca_yBa_{2-y}La_yCu_3O_{7-\delta}$ have been successfully grown [52, 58]. This system has been shown to dramatically reduce degradation in water vapor environments. Substitutions with $y = 0.4$ have a greater than 100-fold increase in lifetime in a corrosive fluid as compared to $YBa_2Cu_3O_{7-\delta}$ [52]. This composition has $T_c = 82$ K, the highest of the doped family.

5.1 Experimental

The TXYBCO growth recipe is a modification of the standard 1-4-10 flux method of growing YBCO crystals. In the standard recipe for YBCO, high purity (99.99% or better) raw ingredients are mixed in a molar Y:Ba:Cu 1:4:10 ratio to produce 6 g of flux mixture. The raw ingredients are Y_2O_3, $BaCO_3$, and CuO. In the preparation of polycrystalline samples, the raw chemicals must be dried for at least an hour before weighing. In the preparation of single-crystal samples, the drying step is not necessary. The flux mixture is not the exact stoichiometric composition of the final product as it is during polycrystalline sample preparation. The error introduced by using undried chemicals is much smaller than the deviation from the stoichiometry of the final product. The flux mixture is calcined at 900°C, ground for an average of five times, once daily. During the calcining, the mixture is held in an alumina crucible. After sufficient grinding, as determined by the experimenter, the flux is divided into two 3 g samples. One of those samples is left in the calcining oven in an alumina crucible. The other is placed in an yttria stabilized zirconia crucible. The yttria stabilized zirconia crucibles introduce fewer contaminants into the crystals than the alumina crucibles do. There is still some contamination as evidenced by flux-pellet-sized and -shaped depressions which develop as the crucibles are used again and again. The pellet of flux is then heated and cooled according to the algorithm illustrated by Fig. 5.1. The flux is first melted at 1000°C, then slowly cooled to room temperature. The slow cooling is essential not just for the crystal growth, but also to avoid breaking the crucible. The crystals grow along the edges of the crucible. Removal must be done with extreme care to avoid breaking the crystals. A scalpel cleaned with acetone is an appropriate tool for crystal removal.

After removal from the zirconia crucible, the crystals must be oxygenated to achieve ideal oxygen content, and thus the highest possible T_c. This is done by placing them in a pure oxygen flow for five weeks at 375°C. The crystals are placed on gold foil and the foil is placed inside alumina crucibles. The gold foil prevents contamination from the alumina. Several batches of crystals may be

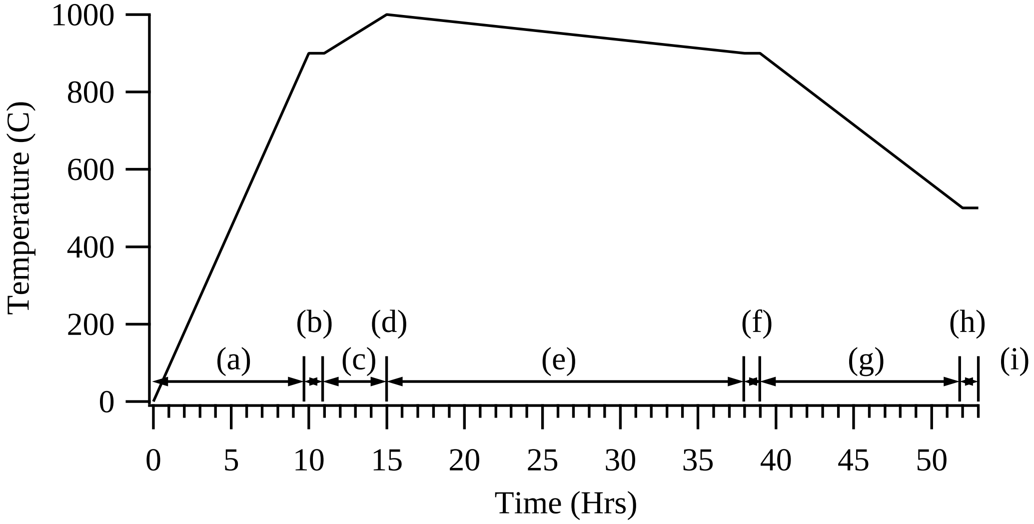

Figure 5.1: Heating recipe for YBCO crystal growth. (a) 10 hr. ramp from room temperature to 900°C (b) 1 hr. soak at 900°C (c) 4 hr. ramp to 1000°C (d) 3 min. soak at 1000°C (e) 23 hr. ramp to 900°C (f) 1 hr. soak at 900°C (g) 13 hr. ramp to 500°C (h) 1 hr. soak at 500°C (i) Oven turns off and cools to room temperature.

oxygenated at the same time. This increases throughput tremendously. A SQUID magnetometer is used to determine if there is a superconducting transition and the temperature of that transition. Ideally, it should be 92 K.

A doped polycrystalline sample was made before any doped single-crystal samples were attempted. The polycrystalline sample served as a reference in later analysis. This sample was made by mixing high-purity Y_2O_3, $BaCO_3$, La_2O_3, Ca_2CO_3 and CuO in a molar ratio of 0.6:0.4:1.6:0.4:3 Y:Ca:Ba:La:Cu. The mix was calcined at 910°C, ground daily for an average of five days. X-ray analysis determined that the reaction had fully taken place. The powder was pressed into pellets, and the pellets were oxygenated at 375°C for 3 days.

Single-crystal samples of doped YBCO were prepared by slightly modifying the method described above. The raw ingrediants now include high-purity La_2O_3 and Ca_2CO_3. Our initial high purity flux composition included Ca and La such that the proportions would be 0.6:0.4:3.6:0.4:10 Y:Ca:Ba:La:Cu. This flux mixture was calcined at 910°C, ground for an average of five times, once daily. The mixture was then placed in an yttria stablized zirconia crucible, melted at 1040°C and slowly cooled to room temperature as shown in Fig. 5.2. The higher melting temperature is used because the flux pellet was frequently unmelted when heated to 1000°C. Longer cooling times were used because the crystals did not grow with a cooling time of 23 hours. Crystals are oxygenated by allowing them to sit in a flow of pure oxygen at 375°C for five weeks, and the transition temperature is measured with the SQUID.

Preliminary energy dispersive spectroscopy (EDS) measurements indicated that the initial flux mixture resulted in crystals with a deficit of Ca and excess La. We took three approaches to modifying the flux mixture to produce crystals with compositions closer to the ideal: 1) increase the amount of Ca, 2) decrease the amount of La, and 3) a combination of these two. EDS spectra were taken at three separate points on each crystal and normalized to the copper peak height. We compared normalized peak heights of all crystals to a stoichiometrically ideal, polycrystalline sample to determine which were closest to the ideal composition. Table 5.1 shows the flux compositions from which all the crystals in this study came.

We immersed samples of both doped and undoped YBCO in deionized water for increasing lengths of time. After each period of soaking, we examined

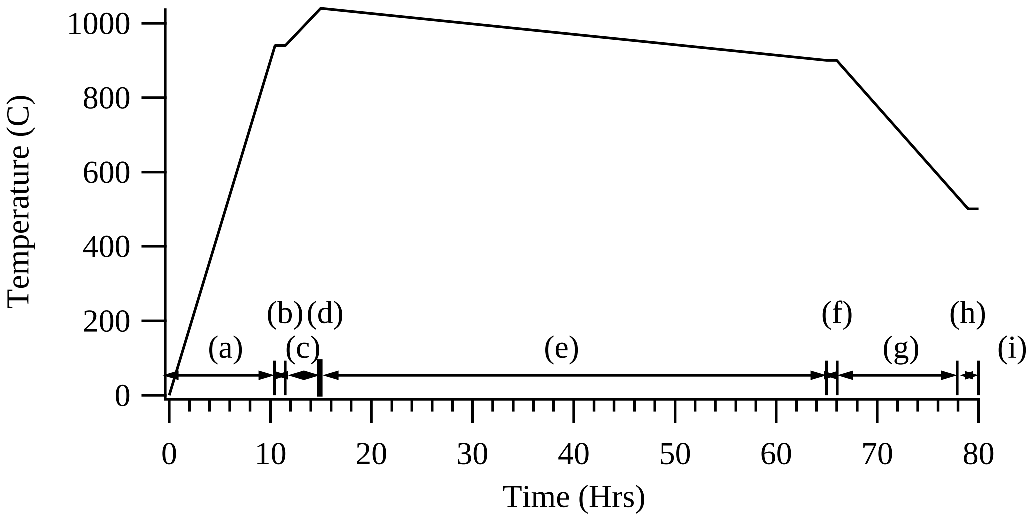

Figure 5.2: Heating recipe for TXYBCO crystal growth. (a) 10.5 hr. ramp from room temperature to 940°C (b) 1 hr. soak at 940°C (c) 3.5 hr. ramp to 1040°C (d) 5 min. soak at 1000°C (e) 50 hr. ramp to 900°C (f) 1 hr. soak at 900°C (g) 13 hr. ramp to 500°C (h) 1 hr. soak at 500°C (i) Oven turns off and cools to room temperature.

the samples with an SEM for evidence of corrosion.

5.2 Results and Discussion

Table 5.1 presents the samples grouped according to the composition of the flux from which they were made. Sample 1 is the polycrystalline ideal to which all others were compared. Samples 2 and 3 are from the initial flux composition (0.6:0.4:3.6:0.4:10 Y:Ca:Ba:La:Cu). Samples 4-7 were grown from a flux with increased Ca as compared to the original. Samples 8 and 9 were grown from a flux with decreased La. Sample 10 was grown from a flux with both increased Ca and decreased La. All samples, with the exception of 6 and 7, were taken from

Table 5.1: Relative amounts of La and Ca in the flux from which the crystals were grown.

Sample	1[a]	2,3[b]	4	5,6,7[c]	8,9	10
La	*	1.0	1.0	1.0	0.5	0.75
Ca	*	1.0	1.1	1.5	1.0	1.5

[a]Polycrystalline [b]Reference flux composition [c]6 and 7 are from the same melt

separate melts. Samples 6 and 7 are from the same melt.

Figures 5.3 and 5.4 present the data from EDS. Figure 5.3 presents the individual peak heights (copper = 1 for all), and Figure 5.4 presents the ratios Ca:Y and La:Ba. Overall, the Ba peak heights show only about a ten percent variation (less, if samples 8 and 9 are excluded) and are centered around the value from the bulk sample. The La, Ca, and Y peak heights all show about a thirty percent variation and are not centered around the bulk values. The La peak heights are consistently high, with the exception of sample 8, as compared to the ideal composition. The Y peaks are consistently low. The Ca peaks are both high and low, but the average is a little low. This may indicate that some of the La is going to the Y site, especially taken together with the observation that the variation in the La:Ba ratio follows the variation in La peak height. The extremely large variation in the Ca:Y peak height may be understood if there is some La reducing the available sites for Y and Ca.

We considered a model of the 1-2-3 system $Y_{1-x-y}Ca_xLa_yBa_{2-w}La_wCu_{3+\epsilon}O_{7-\delta}$ which allows for La to sit on the Y site and for residual CuO flux which may be present on a sample. We assume that the

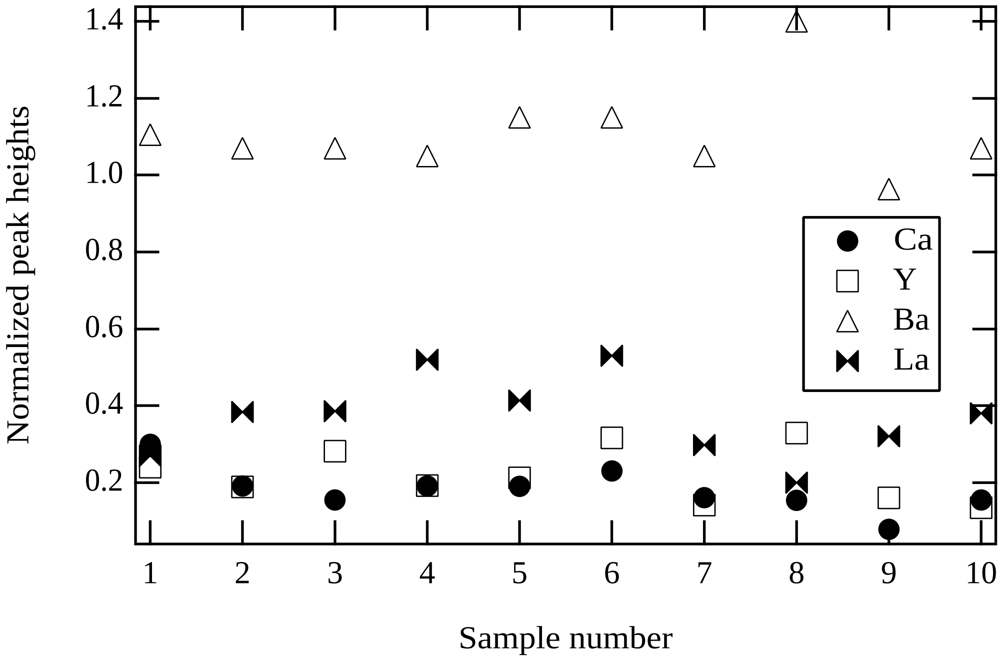

Figure 5.3: Y, Ca, Ba, and La peak heights from EDS spectra. All spectra are normalized such that the Cu peak has a height of 1.

peak height ratios are directly proportional to the subscript ratios with a constant of proportionality which is composition independent. The peak height ratios and the stoichiometric relations in our model system give us sufficient information to find the composition of our single-crystal samples. This model gave good results for most of our nine single-crystal samples. Samples 6 and 8 gave us unreasonably negative values of ϵ. These two samples are also not superconducting. The results for the other seven are in Table 5.2.

Samples 2-7 comprise the series with increasing Ca in the flux (La held constant). Samples 2 and 3, and 8 and 9 comprise the series of decreased La in the flux (Ca held constant). Samples 2 and 3, and 10 comprise the series of both increased Ca and decreased La. Examining the figures, it is difficult to

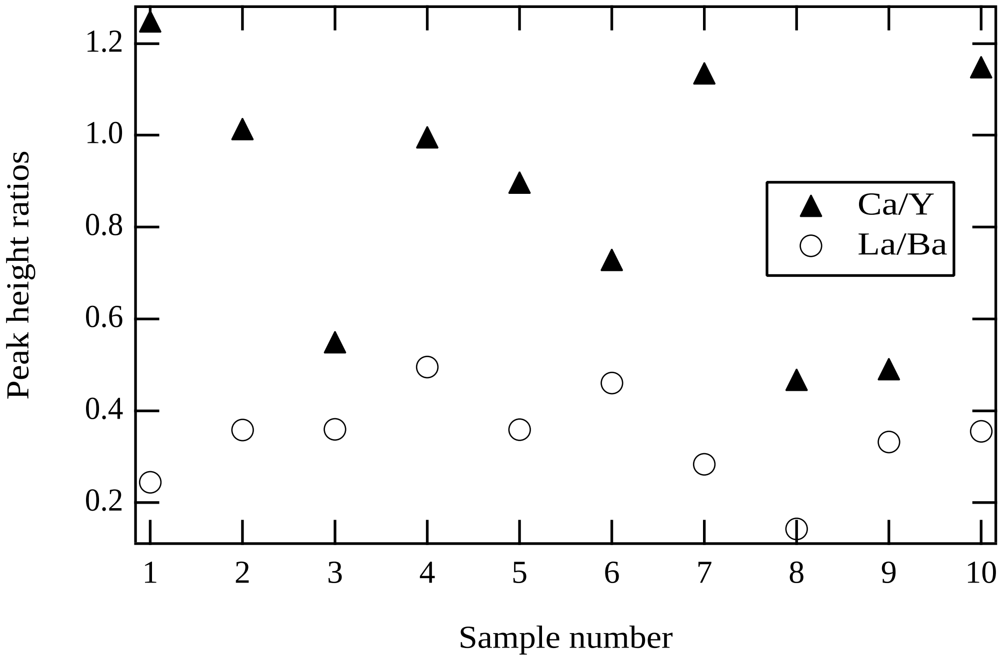

Figure 5.4: Ratios of Ca:Y and La:Ba peak heights from EDS spectra.

distinguish any such systematics in the resulting crystal composition. There is as much variation within the same flux composition (e.g., samples 2 and 3 or samples 8 and 9), and even within the same batch (e.g., samples 6 and 7), as there is between all the flux compositions. It appears that flux composition has a limited effect on the composition of the resulting crystals.

Figure 5.5 shows the irreversibility temperature, T_{irr}, of samples 2–5, 7, 9, and 10 plotted as a function of the peak height ratios (samples 6 and 8 were not superconducting). The irreversibilty temperature is defined as the temperature at which the field-cooled and zero-field-cooled SQUID magnetometry curves begin to show hysteresis. There is some systematic change in T_{irr} which follows the change in La:Ba peak height ratio. There is no such correlation with the Ca:Y peak height ratio. Sample 9 has the highest T_{irr} of the single-crystal samples;

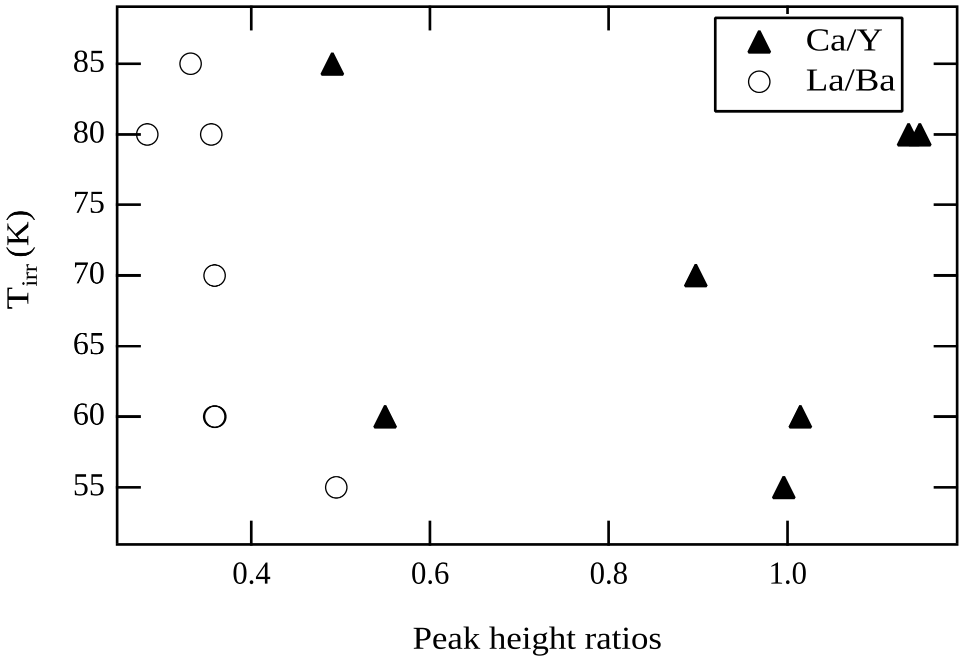

Figure 5.5: Superconductivity irreversibility temperature as a function of Ca:Y or La:Ba peak height ratios from EDS spectra.

higher even than the polycrystalline sample, sample 1. It also has a severely depressed La:Ba peak height ratio as compared to sample 1. Sample 10 and sample 7 have the next highest T_{irr}, and have the ratios which are closest to those of sample 1.

We immersed single-crystal samples of YBCO and doped YBCO in deionized water to test the corrosion resistance. SEM images taken before soaking and after soaking for 28 days are presented in Fig. 5.6 and Fig. 5.7. The two figures have the same scale. The doped YBCO crystal shows increased corrosion resistance as compared to the YBCO crystal even though it does not quite achieve the ideal composition previously determined for polycrystalline samples.

Table 5.2: Composition of samples. Our model of the system gave unphysical values for samples 6 and 8. Those two samples were also not superconducting.

Sample	Composition
2	$Y_{0.50}Ca_{0.27}La_{0.23}Ba_{1.63}La_{0.37}Cu_{3.17}$
3	$Y_{0.70}Ca_{0.20}La_{0.10}Ba_{1.53}La_{0.47}Cu_{2.98}$
4	$Y_{0.48}Ca_{0.25}La_{0.27}Ba_{1.50}La_{0.50}Cu_{2.98}$
5	$Y_{0.52}Ca_{0.25}La_{0.23}Ba_{1.63}La_{0.37}Cu_{2.95}$
7	$Y_{0.42}Ca_{0.25}La_{0.33}Ba_{1.80}La_{0.20}Cu_{3.57}$
9	$Y_{0.49}Ca_{0.13}La_{0.38}Ba_{1.77}La_{0.23}Cu_{3.82}$
10	$Y_{0.38}Ca_{0.23}La_{0.38}Ba_{1.75}La_{0.25}Cu_{3.40}$

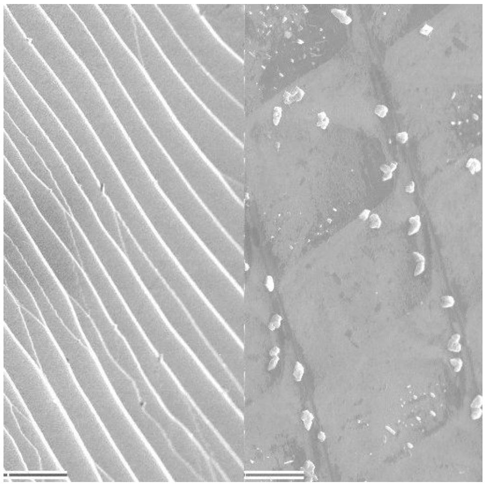

Figure 5.6: YBCO (right) and doped YBCO (left) before soaking in deionized water.

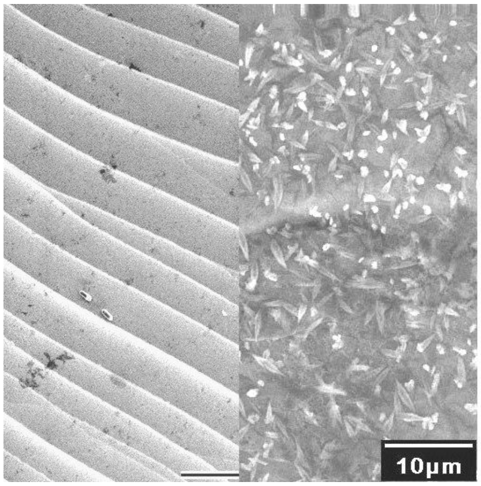

Figure 5.7: YBCO (right) and doped YBCO (left) after soaking for 28 days in deionized water.

Chapter 6

Results, Analysis, and Discussion

6.1 Results

Fig. 6.1 shows typical capacitive, frequency scans of an oscillator, including the lower cantilever (a), lower torsional (b), upper cantilever (c), and upper torsional (d) modes. The scans were taken at room temperature in 200 mTorr of He with $V_{bias} = 250$ V. $V_{drive} = 10$ V in a) - c), and 1 V in d). These scans enable an evaluation of the simple models presented in Sec. 2.4. The resonant frequencies for these scans are a) $f_o = 1810.6$ Hz, b) $f_o = 2111.6$ Hz, c) $f_o = 7031.6$ Hz, d) $f_o = 11396.08$ Hz. These values are within 15-20% of the values predicted by Eqns. 2.15 and 2.32. The frequency ratios are

$$\frac{\omega_{ut}}{\omega_{lt}} = 5.3969 \tag{6.1}$$

$$\frac{\omega_{uc}}{\omega_{lc}} = 3.8836 \tag{6.2}$$

in very good agreement with predictions of 5.5 and 3.8, respectively. The discrepancy in the values of the resonant frequencies can be partly explained byt

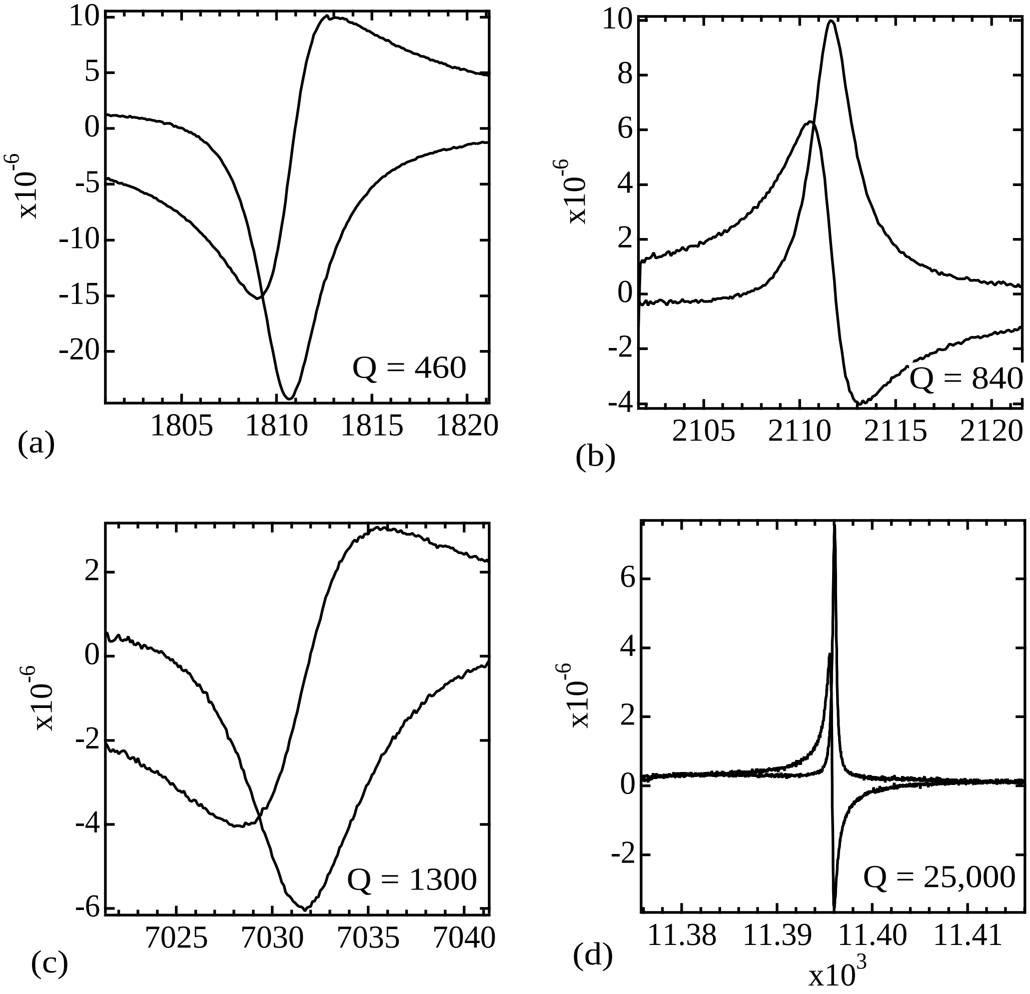

Figure 6.1: Frequency scans of an oscillator. a) lower cantilever b) lower torsional c) upper cantilever d) upper torsional. The x-axis spans 20 Hz on all graphs for ease of comparison. The Q of each mode is noted on the graph. All data were taken with a 10 V drive, except for d), which was taken with a 1 V drive.

the simplicity of the model. However, process induced variations in the size and especially the squareness of the oscillators produce variations in the resonant frequencies of the same order as the variation between the prediction and the measurement.

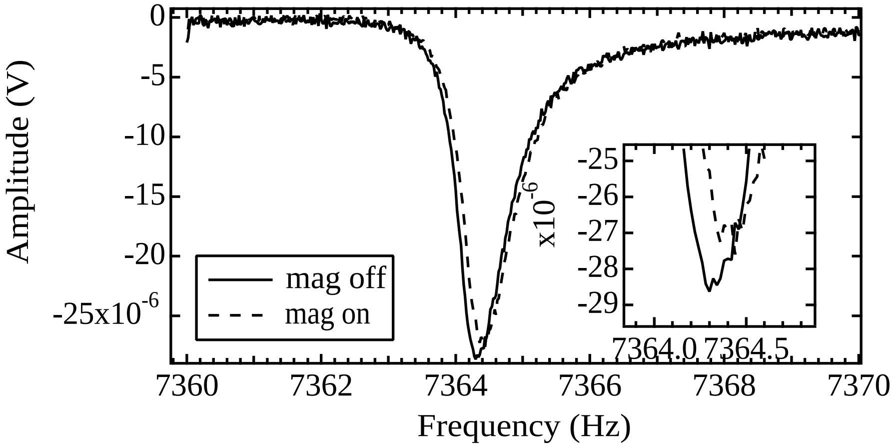

Figure 6.2: Capacitive sweep of the uppercantilever mode with magnet on and off. Only the absorptive amplitude is shown. Inset: A magnified view of the peak, showing more clearly the shift in resonant frequency. 2 V drive, 250 V bias, 77 K.

The absorptive amplitude from a capacitive sweep of the upper cantilever mode with the magnet on and off is shown in Fig. 6.2. This figure illustrates the change in resonant frequency in the presence of additional forces that was discussed in Sec. 2.4. The frequency shift in this mode is very small and can be hard to verify. The inset in Fig. 6.2 shows the shift more clearly.

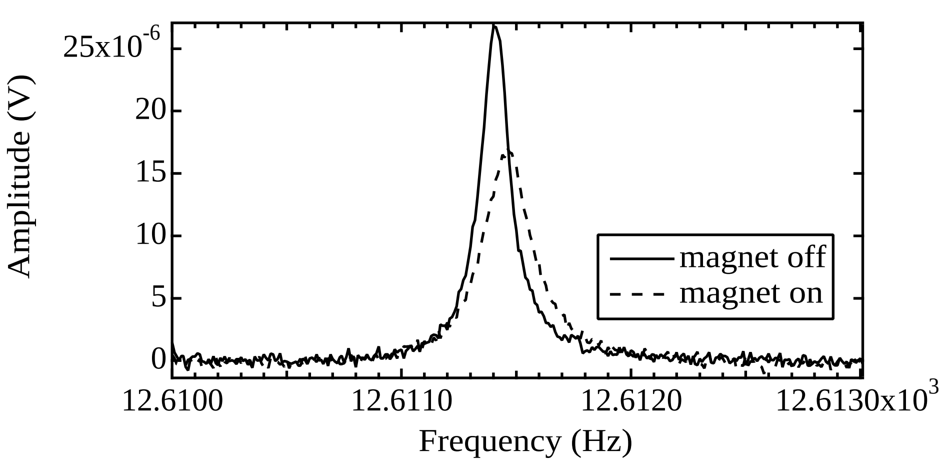

Figure 6.3: Capacitive sweep of the upper torsional mode with magnet on and off. Only the absorptive amplitude is shown. 1 V drive, 250 V bias, 77 K.

Figure 6.3 shows a capacitive sweep of the upper torsional mode with the magnet off and on. The frequency shift is very obvious in this mode. Eqn. 2.25 indicates that the frequency should be lower in the presence of viscous forces. The shift to higher frequency indicates that there is some residual pinning. The decreased peak height and increased peak width are a result of dissipation. The change in Q may be used to find the dissipation coefficient, η. For the damped, driven oscillator in Eqn. 2.2, the dissipation coefficient is

$$\eta = \Gamma M, \tag{6.3}$$

which can be related to the Q via

$$Q = \frac{\omega}{\Gamma}. \tag{6.4}$$

We make the approximation that $\omega_v = \omega_o$. This is a valid approximation because the frequnecy shift is expected be a few parts in 10^6. The increase in Γ which can be found from the decrease in Q yields the dissipation coefficient per unit length per vortex

$$\eta = 3.35 \times 10^{-6} \tag{6.5}$$

A capacitive sweep of the upper cantilever mode, in which the wing is driven capacitively with the magnet off, is shown in Fig. 6.4a. The conditions for this sweep are $V_{bias} = 250$ V, $V_{drive} = 2$ V. A viscous sweep is shown in Fig. 6.4b-c. The dashed lines are sweeps with the magnet on with field in the positive and negative directions. The solid lines are sweeps with the magnet off, showing the residual motion from the coupling to the moving piezo stack. These graphs can be used to calculate the value of the dissipation coefficient. For these data, $d_{gap} = .03048$ cm. We can estimate the force experienced by the oscillator from the amplitude of the detected signal in Fig. 6.4a using Eqn. 3.1

$$F = \frac{C_{gap} V_{bias} V_{drive}}{d_{gap}} = 1.89 \times 10^{-6} \text{ N}. \tag{6.6}$$

Recall that this force is on the wing. The amplitude from Fig. 6.4a is $A_{ab} = 28.63$ μV, $Q = 8000$. Rewriting Eqn. 3.6 gives

$$\frac{F}{A_{ab}} = \frac{k}{Q} = 6.6 \times 10^{-8} \ \frac{\text{N}}{\mu\text{V}} \tag{6.7}$$

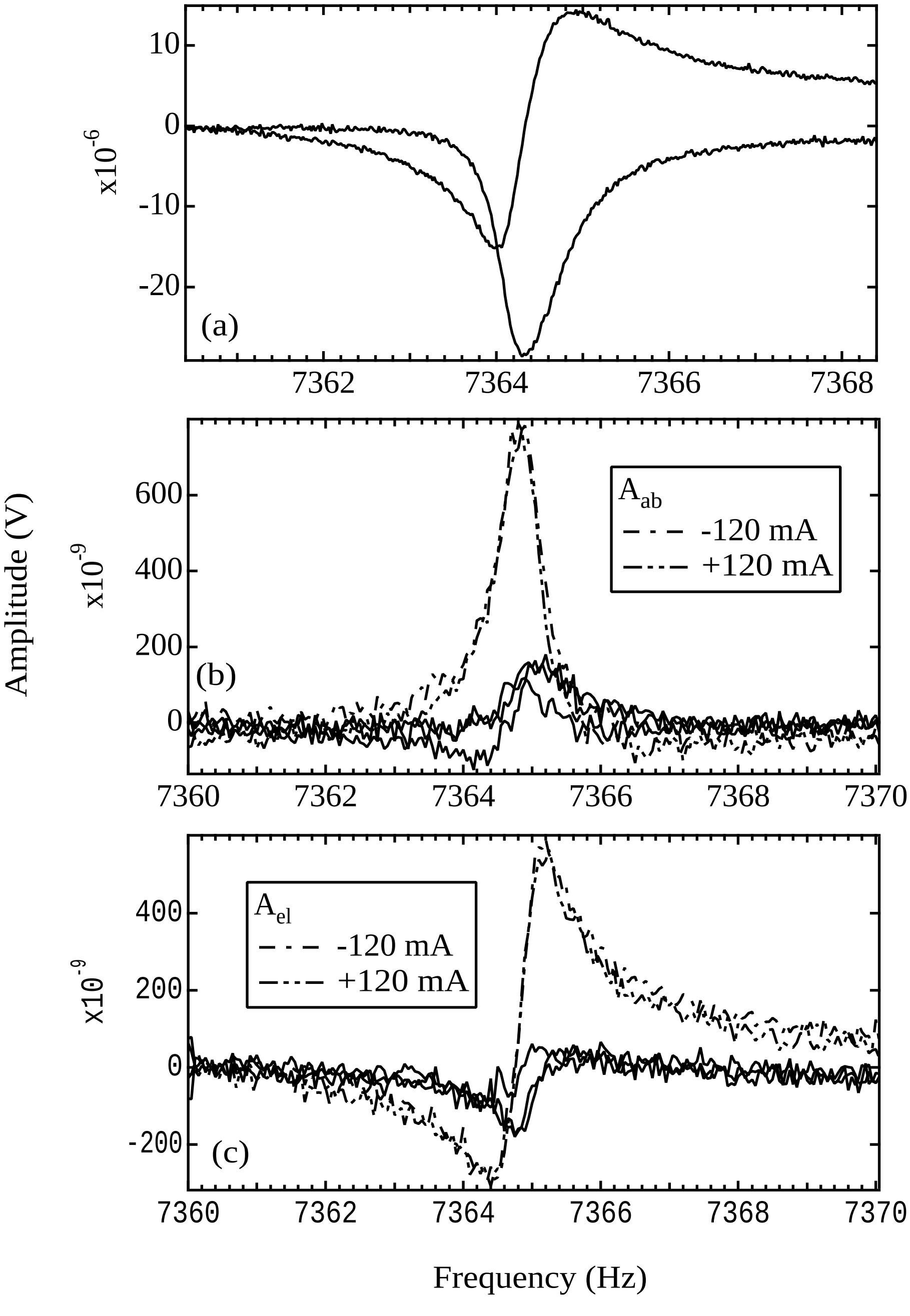

Figure 6.4: Data taken at 77 K in 200 mTorr He using upper cantilever mode. a) Capcitive sweep, 2 V capacitive drive, 250 bias, magnet off. b)-c) Viscous sweep, 10 V magnet drive, 250 V bias. Solid lines are magnet drive with no field.

The amplitude from Fig. 6.4b is $A_{ab} = .771\ \mu\text{V}$. We may again use Eqn. 3.6 with the result found in Eqn. 6.7. The result in Eqn. 6.7 is from a drive on the wing. To acheive the same wing motion with a drive on the head, we must use the conversion factor found in Eqn. 2.35.

$$F_{visc} = A_{ab}\frac{k}{Q} = (6.6 \times 10^{-8}\ \frac{\text{N}}{\mu\text{V}})(.56)(.771\mu\text{V}) = 2.85 \times 10^{-8}\ \text{N} \tag{6.8}$$

The viscous force is expressed in Eqn. 1.24

$$\vec{F}_{visc} = -\eta\vec{v}. \tag{6.9}$$

This can be expressed in terms of magnitudes and solved for the dissipation coefficient, η. The quantity we are interested in is the dissipation coefficient per vortex per unit length:

$$\eta = \frac{v}{F_{visc}}\frac{1}{(\#\text{ of vortices})(\text{thickness of crystal})}. \tag{6.10}$$

The number of vortices was estimated in Sec. 3.3 to be 1.54×10^7. The velocity of the vortex is easy to find. The magnet moves 12.7 nm at 7364.3 Hz,

$$v_v = A_v 2\pi f_o = 5.8 \times 10^{-4}\ \frac{\text{m}}{\text{s}} \tag{6.11}$$

The thickness of the crystal is calculated from a measurement of the area and the mass,

$$t = \frac{m}{\rho l w} = \frac{1.718 \text{ mg}}{(7 \text{ g/cm}^3)(.1778 \text{ cm})(.254 \text{ cm})} = 5.4 \times 10^{-3} \text{ cm}. \tag{6.12}$$

With these values, we find

$$\eta = 5.8 \times 10^{-7} \, \frac{\text{g}}{\text{cm-s}} \tag{6.13}$$

In Sec. 1.7. we estimated the dissipation coefficient to be

$$\eta = 8 \times 10^{-7} \, \frac{\text{g}}{\text{cm-s}}. \tag{6.14}$$

The differences in the values in Eqns. 6.5, 6.13, and 6.14 may be attributed partly to uncertainties in measuring physical properties, and partly to simplicity of the models involved. The thickness of the crystal is not always uniform across its area. The crystal is given to cleavage, and it does not always cleave cleanly across the sample. It also tends to fall off the oscillator entirely, leaving a small piece behind. The thickness which we calculate is an average thickness, and may not represent the exact value at the spot where the vortices penetrate. The area of the crystal is not a perfect square. The oscillators are difficult to measure, as the polished face is smaller than the unpolished face. The oscillators exhibit significant variation in squareness, which is not accounted for in the simple model we use to predict the resonant frequencies. The values which we took from the literature may not be exact for our sample. For example, $H_{c2} = 7.5$T is based on a sample whose transition temperature is 87 K. The midpoint of the superconducting transition shown in Fig. 3.2 is closer to 80 K. The expressions Eqns. 6.3

and 6.4 are based on a single oscillator model, when in fact, we use a double oscillator. The Bardeen-Stephen model is also very simple. With this in mind, there is reasonable agreement between the value in Eqn. 6.13 and that in Eqn. 6.14.

6.2 Summary and Future Work

We report the value of the dissipation coefficient at 77 K. Further work should include temperature dependant measurements of the dissipation coefficient. In particular, the location of the pinning-viscous transition is of interest. Further studies should include amplitude-dependent measurements to verify $F_{visc} \propto v$, and measurements with different crystal thicknesses to examine possible thickness effects.

Appendices

Appendix A

Running the Experiment

This chapter details the actual running of the experiment. The experiment may be run in two modes: measuring a resonance and measuring a force. The difference is a question of changing two connections.

A.1 Equipment

All the electronic equipment needed for the experiment is mounted on one rack. The equipment is:

Main Control box

Kikusi Electronics Corporation COS6100M Oscilloscope 100 MHz

Hewlett Packard 3325B Function generator

Conductus LTC-20 Temperature controller

Stanford Research Systems SR530 Lock-in amplifier

Fluke 8000A Digital multimeter

Acopian Current/Voltage source (3)

Fluke 5440B/AF High voltage source

Piezo control box

Offset control box

Diode protection boxes (2)

The first item and last three items are homemade and are labeled for identification. The following sections detail the use of each piece of equipment individually. When running the experiment, the electronics are all used together. The following sections should be used as reference when trying to understand the experiment as a whole, as described below.

In addition to the rack-mounted electronics, this experiment uses a Janis dewar, the blue pump station, a Macintosh IIci to take data using Labview ("Dewey"), another Mac IIci to plot data using Igor ("Sally"), and of course, the probe. Two computers are necessary as Dewey cannot run Igor and take data with Labview simultaneously.

A.1.1 Oscilloscope

The scope is used to view the piezo drive and capacitive cancellation signals when measuring a force. It is not necessary when measuring a resonance. The piezo drive signal comes out of the piezo control box from the port labeled "fixed 0". This signal may be viewed on Ch. 1 of the scope. The capacitive cancellation signal also comes from the piezo control box, from the port labeled "out". It may be viewed on Ch. 2. The connections from piezo control box to scope do not need to be changed if the scope is only used when measuring a force. When measuring a resonance, the scope has no input and there will be nothing on the screen.

A.1.2 Function Generator

The function generator (FG) provides the sinusoidal drive signal for all measurements (resonance and force). The FG has a maximum output of 10 V peak to peak. Be warned: if you look at this signal on the scope, it will in fact be 10 V zero to peak. This mislabeling should be kept in mind at all times. The output will come from the port labeled "Main Signal". There will be two outputs, so a T-connector is necessary. One output will never change. This output goes from "Main Signal" to "Input" on the lock-in. The other output will be changed depending on the measurement being made.

When measuring a resonance, the second output goes from "Main Signal", through the diode box labeled "1", to port 2 on the probe. This is the drive signal to one of the electrodes. The output from the FG may be any value up to 10 V, although too strong of a drive is undesirable.

When measuring a force, the second output goes from "Main Signal", through the diode box labeled "1", to the port labeled "in" on the piezo control box. This is still the drive signal, but now the piezo is being driven rather than the oscillator. A 2 V peak to peak drive signal is used for force measurements. This is amplified 5X into a 10 V peak to peak signal which drives the piezo. Less is okay, more will cause irregularities in the output sine wave.

A.1.3 Lock-in Amplifier

The lock-in has two inputs: reference and signal. There is one reference input port. The output from the FG goes into the reference input. There is another connection to the reference input, which is from the offset control box, from the port labeled “in”.

There are three input ports on the signal input, only two of which are used. The port labeled “B” is connected to the “out” port on the offset control box. The port labeled “A” is connected through the diode box labeled “2” to port 3 on the probe. This is the pickup. The switch above the ports should be in the “A-B” position.

The lock-in can tell you if the oscillator has broken. Flip the switch to “A”, remove the “B” input. At room temperature, with a 10 V drive signal, Ch. 1 of the lock-in should read approximately 10-15 μV. When the oscillator is broken, the offset will be much higher. Remember to flip the switch back and reconnect “B”.

There is no need to change the connections on the lock-in (except to check for a broken oscillator).

A.1.4 Offset Control Box

The offset control box (also called the A-Φ box) is used to cancel any electrical offsets from the signal. It is connected as described above, with the “in” port connected to the reference input on the lock-in and the “out” port connected to the “B” signal input on the lock-in. The circuit diagram is on the inside of the lid to the box.

The offset is a function of many things: the drive voltage, the frequency, the temperature, the position of the many cables. It is canceled with the “AMP” and “Φ” knobs and the “INV” switch on the front of the box. It sometimes takes great perseverance to actually cancel the offset. One should avoid moving any cables after it is canceled as that will change the offset.

A.1.5 High-voltage Generator

The output of the high-voltage (HV) generator is the top pair of banana plugs on the left. It is connected, through a BNC-to-banana adapter, to port #1 on the probe.

The settings for the HV generator are: current: .1 mA limit; voltage: high limit +250 V, low limit -0 V.

The “OPR/STBY” button changes the HV generator from operate mode to standby mode. The generator should be left on standby when connecting or disconnecting leads. The generator should be put on standby and disconnected when working on the interior of the probe.

A.1.6 Piezo Control Box

The piezo box is used only when measuring a force. It has many input/output ports, which can be very confusing. The circuit diagram is on the inside of the lid. The box has capability to excite all four of the piezo quadrants. It is generally used only to excite two at a time to excite motion parallel and perpendicular to the oscillator.

The piezo box has two functions. It controls the motion of the piezo, and it sends a capacitive signal to the oscillator. The point of the capacitive signal is to cancel mechanical coupling from the piezo to the oscillator. More on this is in Sec. A.4.

The front of the piezo box has four potentiometer knobs, two switches, and a third on/off switch. The four knobs and two switches control the capacitive signal sent to the electrode which drives the oscillator. The controls are amplitude port 1 (knob), phase port 1 (knob), invert port 1 (switch), amplitude port 2 (knob), phase port 2 (knob), invert port 2 (switch). In general, only one port is used at a time, say, port 1. This makes everything much simpler. The amplitude knob controls the amplitude of the signal sent to the electrode. The phase knob controls the phase of the signal sent to the electrode with respect to the phase of the signal sent to the piezo. This is why both signals are viewed on the scope (see A.1.1). The phase knob can only go 180°. The invert switch inverts the signal, allowing a full 360°. The invert switch on port 1 is labeled + and -. The capacitive signal is referred to in the author's lab notebooks as +0 to +180° or -0 to -180°. A note of +72° means, for example, that the capacitive and piezo drive signals are 72° apart, with the invert switch in the + position.

The back of the piezo box has six BNC ports. The is an "in" and an "out", which are obvious. The others are inexplicably labeled "port 2 0", "port 2 180", "fixed 0" and "fixed 180". Assuming only two piezo quadrants are being driven at once, the interesting ports are "fixed 0" and "fixed 180". The "in" port is attached through the diode box labeled "1" to the "main signal" output on the FG. This connection is only made during a viscous sweep. There is no input to the piezo box during resonance sweeps. The "out" port of the piezo box is connected to “2” on the probe. This is the drive electrode for the oscillator. Its use will be described below. The “out” port is also connected to Ch. 2 on the scope. The “fixed 0” and “fixed 180” are connected to the piezo tube. In measuring a viscous (longitudinal) force, “fixed 0” is connected to “B” and “fixed 180” is connected to “D” on the probe. The names become slightly more clear at this point, as the two quadrants of the piezo are driven with signals 180° out of phase with each other. “Fixed 0” is also connected to Ch. 1 of the scope.

Except for the input to the “in” port, all connections may be left in place at all times. When you are ready to drive the piezo, connect the input. When not driving the piezo, leave the input unconnected.

A.1.7 Digital Multimeter and Current/Voltage Source

The digital multimeter (DMM) is used with one of the current/voltage sources to provide current to the electromagnet. The DMM is used as an ammeter. To put current through the magnet, first turn up the current on the current source. Then turn the voltage up while reading the DMM. Turn up the voltage until you read 200 mA, then turn down the voltage until you reach 120 mA, or whatever your desired current is. Turning the current up to 200 mA first serves to destroy any hysteresis.

A.1.8 Current/Voltage Sources

The other two current/voltage sources provide power to the offset control box, the piezo control box, and the main control box. They should have an output of 0 Amp. and 15 V.

A.1.9 Temperature Controller

The probe has a thermometer on it, and the Janis dewar has a thermometer and a heater. The temperature controller can monitor the temperature of both the probe and dewar, and control the temperature of the dewar when it is filled with cryogenic fluids. The controller has two inputs in the back- one for each thermometer – and an input for the heater control. Sensor 1 is for the thermometer on the dewar. There is a special cable to connect the two. This cable is a doubled cable, with the connector for sensor 1 on the end of one cable, and a black connector for the heater on the other cable. Both these cables have a distinctive 7-pin connector at the other end which plugs into the dewar. Sensor 2 is for the thermometer on the probe. This is also a doubled cable, but only one cable is used. The other end is a 10-pin connector which goes through an adapter to a 5-pin connector on the main control box.

Sensor 1 should be set to 1945, and sensor 2 should be set to 2501. Sensor 1 will not read above approximately 266 K. For full instructions in the use of the controller, see the manual.

A.1.10 Main Control Box

The main control box is labeled “Vortex Control Box”. It is sometimes referred to as the “mystery box” as much of its functioning is unrecorded, and therefore unknown. It’s creator did not leave a circuit diagram, and the electronics shop was unable to construct one. There are some controls on the front of the box, but it is not clear exactly what they control. The most important function of this box is to provide electrical connections for the thermometer, electromagnet, and pick-up coil on the probe. There is a 24-pin cable which goes from probe to the box. Pins E, F, H, and J are connected to the thermometer on the probe. Their mates on the control box are fed through to a 5-pin connector, into which the cable to sensor 2 on the Conductus is plugged. Pins Y and Z go to the magnet coil on the probe. Their mates on the control box are connected to some screw connectors which are labeled "coil". The wiring which leads to the DMM and current source is screwed down in these connectors. Pins K and R go to the pick-up coil on the probe. Their mates on the control box are fed through to a BNC connector, which is labeled "pick-up". This output is used to view the current in the pick-up coil. Using the pick-up coil takes some ingenuity and fancy wiring, as an ac current must be sent through the main coil to see anything at all. The main control box also has a place to mount a vacuum gauge.

There are many other pins and connectors, but they are unused, or their use is unknown.

A.1.11 Computer Control

The computer which contains the National Instruments card and the Labview program is Dewey. The version of Labview is Labview 2. The Labview program is called "freq sweep lock-in w/ plot" and is found in the folder
Dewey:LabVIEW:Koki's LV files.

Dewey and Sally should be networked to each other, but not to any of the other machines. Networking to the other machines slows down Dewey unnecessarily. All the data is currently stored on Dewey. Sally is used to make Igor plots of scans. When actually taking data, each scan can be plotted while the next is being taken.

A.2 Set-up

Running the experiment requires that an oscillator be in place, a crystal be mounted on the oscillator, and the magnet aligned around the crystal. This section describes how to do all of these things.

A.2.1 Testing the Oscillator

The first step is testing the oscillator. Pick an oscillator, preferably one which has not already been determined to be bad. Place it in the clamp in the probe so that the metallized side faces the electrodes. Screw down the clamp as tightly as it will go. If the oscillator is held only loosely, the Q will be terrible. Carefully move the electrodes close to the wings. Move each electrode the same distance away from the wings, and measure and record that distance. Solder the lead on the oscillator to the blue wire.

Now seal the probe. Use the lead solder on the green spool as an o-ring. (Be sure to remove any solder remaining on the probe from the last seal.) Place the vacuum can on the probe so that the scratches on the can match up with the scratches on the collar. It is very important to seal the probe in the same alignment each time. Use new screws each time you seal the probe[1]. Likewise, grind down the head of the Allen wrench to get sharp corners. Both the screws and the wrench get chewed up with each use, and both must be replaced. Seal the probe by tightening each screw in order in a circular pattern. Do not use a

---

[1] 4-40 ss cap screws available in packs of 100 from Austin Bolt

star pattern. Continue to tighten the screws until they will not move any further. Try not to chew up the heads.

Attach a vacuum pump to the top of the probe and pump down. After pumping for a while, tighten the screws again. Pump for at least a few hours. Overnight pumping is not really necessary at this point.

Refill the probe with 200 mTorr of dry helium gas. To do this, you need two valves in your pump arrangement: one valve between the helium inlet and the vacuum hose, and one valve between the vacuum pump and the vacuum hose. Close the valve on the probe. Close the valve on the pump. Open the valve on the helium and fill the vacuum hose. Close the valve on the helium. This is very important – never pump directly on the helium cylinder. Next open the valve on the pump and pump the hose down. Repeat this once or twice to clean all the air out of the hoses. Then close the valve on the pump, open the valve on the probe, and open the valve on the helium. The probe will fill with helium. Close the valve on the helium, and open the valve on the pump. You are now pumping on the probe. When the pressure drops to 200 mTorr, close the valve on the probe. This takes some practice.

Now that the probe is filled with He gas, turn off the pump and measure a room temperature resonance (Sec. A.3). Try to find all the resonances for completeness. Next place the probe in a bucket dewar of LN2. Allow approximately 1-1.5 hr. for the probe to stabilize at 77 K. When it is stable (as measured on the Conductus), measure a low-temperature resonance. You will have to adjust the pressure at it will have changed from 200 mTorr. Again, try to find all the resonances. The upper torsional mode is very difficult to find at low temperature.

If the Q for the upper cantilever mode at 77 K is 8000 or better, the oscillator is a good one, and you may go on to the next step. Otherwise, test a new oscillator.

A.2.2 Mounting the Crystal

The previous graduate student would mount the crystal on the probe while the oscillator was still in the probe. I have found it much easier to remove the oscillator. Removing the oscillator always introduces the opportunity to break it, however, leaving the oscillator mounted does not guarantee its safety.

With the probe at room temperature, open the vacuum can (if it is sealed). Unclamp, unsolder, and very carefully remove the oscillator. Go to a clear area on a workbench. Collect superglue, acetone, a vacuum tweezers, a glass microscope slide, and a sharpened Q-tip. Determine the alignment of crystal to oscillator. The crystals generally have a raised edge along one side. It is impossible to align the magnet around this edge, so it must go towards the electrodes, or the shiny side of the oscillator. Use the vacuum tweezers to place the crystal on the slide. It should rest flat on the slide, so it is best if the raised edge is up. Use the sharpened Q-tip to place a very small drop of superglue on the sawed off edge of the oscillator head. If you get too much on and make a mess, clean it up with acetone and try again. Turn the oscillator (with glue) upside down and touch it gently but firmly to the crystal. Lift the oscillator – the crystal should stick to it, not the slide. Let dry a second or two, and examine to ensure that crystal and oscillator are at 90° to each other. If the crystal sags, touch the whole arrangment gently but firmly to the glass slide while keeping the oscillator at 90° to the slide. Hold a second or two. Lift the oscillator and examine again.

If the crystal sticks to the slide instead of the oscillator, you have probably used too much glue. Or, it could be that the crystal has thinned. In this case, soak the crystal off the slide using acetone. Let the crystal soak a little, swirling the acetone, to clean it completely. Remove it from the acetone. Place another drop of glue on the head of the oscillator. Leaving the oscillator head up, pick up the crystal with the vacuum tweezers and place it on the oscillator. Leave it a second or two, and make certain that crystal and oscillator are mutually perpendicular.

Remount the oscillator in the probe, resolder, reseal with a new o-ring and new screws, and pump down for several hours. Measure a room temperature and a low temperature resonance as before. The Q will be lower with the crystal mounted, but it should not be significantly lower. If the Q falls dramatically, open the probe and remount the crystal. The crystal adds an unbalanced mass to the oscillator, and the weight distribution has a large effect on the Q. Mounting the crystal is a trial and error process – it is not clear how a particular alignment of crystal to oscillator will affect the Q.

Note: Once the crystal is mounted, keeping the probe under vacuum is of paramount importance. BSCCO, like all copper-oxides, is very sensitive to water in the air. If left exposed to air, the crystal will degrade and will no longer be a superconductor.

A.2.3 Aligning the Magnet

The electromagnet is shaped like a C with a very small gap between the poles. The magnet must be aligned such that the crystal is between the poles, the magnet is not touching either the crystal or the oscillator, and the poles are not near the edge of the crystal. Alignment is done via three arms which attach to the top of the piezo tube. There are two arms for x-y adjustment, and one arm for z adjustment. The arms are adjusted by loosening the screws, moving the arms, and retightening the screws. This maneuvering is extremely tricky and should be attempted only with the greatest caution. The screws which fasten the arms in place are very snug. Loosening or tightening a screw will cause the arm to which it attaches to move. The arms can be held in place by gently grasping them with a pair of tweezers.

Once the magnet is aligned around the crystal, reseal the probe and pump down. At this point, you should take great care with the seal and pump down overnight. If the alignment has gone well, your next step is to take data. Test the resonance at room temperature and low temperature. The trick to aligning the magnet is that it must stay aligned at 77 K. Frequently a good room temperature alignment job is not so good once the probe is cold. If the Q with the magnet aligned is lower than the Q without the magnet, then the probe must be warmed up and the magnet must be realigned. There is no way to predict whether the magnet will stay aligned at 77 K. It is a trial and error process, much like mounting the crystal.

If the alignment is good at 77 K, then it is certainly worthwhile to try to take data as long as the probe is cold.

A.2.4 Transferring the Probe to the Janis Dewar

Measurements at temperatures other than 77 K require temperature control, and this is where the Janis dewar enters the picture. The tricky part is getting the probe into the dewar without breaking the oscillator or shaking loose the crystal. The process takes two people. The dewar is fairly tall, as is the probe. To lift the probe high enough to clear the top of the dewar, you must stand on the aluminum structure which holds the dewar. Fasten the probe as high as it can safely sit on its stand. Have someone loosen the clamps on the probe stand and steady the bottom end while you hold the top end. Slowly and carefully lift the probe until the bottom end clears the top of the dewar. In the mean time, watch the top end so that it doesn't hit any lights or pipes. Carefully put the probe into the dewar and slowly lower it down. Do not lower it the full length of the probe. There is a quick connect and a clamp at the top of the probe. These may be tightened to support the probe slightly above the top of the dewar.

Test the resonant frequency and Q again to make sure the oscillator and crystal survived intact. If they did, you are ready to cool the dewar and take data at different temperatures.

A.3 How to Measure a Resonance

The first step to measuring anything is to connect all the equipment as described above, and turn everything on. This should not be difficult, as all the cables used in this experiment are labeled with what they should be plugged into. Remember that the FG has two possible configurations depending on whether a force or a resonance is being measured. This section assumes that an oscillator is already in place, the probe is pumped down, and the temperature is stable, as described in Sec. A.2. There are four main resonances, as described in Sec. 2.3. The one which is used to take data is the upper cantilever mode, with frequency between 6500 and 7500 Hz, generally in the 6800-7200 Hz range.

A.3.1 Room Temperature Measurements

Set the FG with a 10 V p-p (which is really zero to peak) output, and 6500 Hz (or whatever is most pleasing). Use the amplitude and phase knobs on the offset control box to zero the offset on both Ch. 1 and Ch. 2 of the lock-in. Zeroing both simultaneously is tricky, but possible. Manually scan the frequency in 1 Hz steps. Holding down the up-arrow button on the FG is sufficient. Watch the dials on the lock-in for the resonance. You may have to periodically re-zero the offset, but you do not want to make the mistake of re-zeroing it in the middle of a resonance. As you cross the resonance, the needles on the lock-in will move in the characteristic resonant pattern, as shown in Fig. 6.1. When you find the resonance, watch what the peak amplitude of the absorptive part is. To avoid inducing microcracks in the oscillator, adjust the drive voltage on the FG so that the response is no greater than 10 μV. Manually take .1 Hz steps to find the peak of the absorptive amplitude. Make an estimate of the width of the resonance, as well. A good oscillator will have a width of around 6 Hz at room temperature. If the width is very large, say, greater than 10 Hz, then either the oscillator is very bad, or something inside the probe needs to be adjusted (See Sec. A.2). At room temperature, you want to scan 10 Hz to either side of the resonant frequency. Set the FG to 10 Hz below the resonant frequency. Observe the reading on the lock-in. Set the FG to 10 Hz above the resonant frequency. Observe the reading on the lock-in. Adjust the offset with the offset control box so that on either side of the resonance, the offset will be zero. If the offset changes significantly across the scan, as it will across a 20 Hz scan, adjust it so that the offset is above zero on the high side by the same amount that it is below zero on the low side. This is most important on the channel which measures the absorptive amplitude, as this is the amplitude from which the Q is measured. When you have set the offsets to your liking, go to the computer and plug in the start frequency and end frequency in the appropriate input boxes. The frequency step should be .1 Hz or less. Double check the file name and the folder where the file will be stored. Click on the run button. When the scan is finished, open the file in Igor and plot it. A good scan looks like the one in Fig. 6.1. Measure the resonant frequency and the Q. The next step is measure the Q at low temperature.

A.3.2 Liquid Nitrogen Temperature Measurements

The Q is much higher at 77 K than it is at room temperature. The response of the oscillator will be larger, and the width of the absorptive peak will be smaller. To accommodate this, the drive from the FG and the scanning step size in Labview should both be smaller. They should usually be stepped down by an order of magnitude. If the drive and step size are 10 V and .1 Hz at room temperature, they should be 1 V and .01 Hz at 77 K. The resonant frequency will be higher. To find it, start at the room temperature resonant frequency and manually scan upwards using .1 Hz steps. When the resonance is located, follow the steps above, with the exception that it is only necessary to go 3 Hz above and below resonance (6 Hz total scan). If the Q is good at low temperature, the next step is to move on to force measurements.

A.4 How to Measure a Force

Vortices only exist when the BSCCO crystal in the superconducting state. All measurements will be made at low temperatures, so the drive, etc., comments in Sec. A.3.2 apply.

To measure forces, first make all the connections on the piezo box. Measuring a force is the last step in the data taking process, and follows considerable work on the probe, and many resonance measurements. It is very easy to forget to connect the piezo drive to the piezo. The lead from the drive electrode will be removed from the FG (leaving diode box 1 in place) and reconnected to the "out" port on the back of the piezo box. The output from the FG will no go to the "in" port on the back of the piezo box. All other connections remain as they were. Use no greater than a 2 V drive from the FG. This is amplified within the piezo box to a 10 V drive, and this should register on the oscilloscope. The other signal on the oscilloscope is the drive from the piezo box to the oscillator.

A.4.1 Piezo-Oscillator Coupling

When measuring a force, the piezo tube will be driven. The oscillator has some vibration isolation, but mechanical coupling to the piezo motion is still an issue. To measure the coupling signal, turn the amplitude of the signal from the piezo box to zero. Make sure the current to the magnet is turned off. Scan across 6 Hz. Plot the data in Igor. The response you will see will be some mixture of the absorptive and elastic amplitudes, with amplitude much smaller than the resonance signal. This represents the motion of the oscillator in response to the coupling "drive". This coupling signal is much bigger than any signal which could be produced by vortex motion. The motion of the oscillator is canceled by sending a capacitive, counter-balancing signal of the appropriate phase and amplitude into the drive electrode. This signal is generated within the piezo box, and is viewed on Ch. 2 of the scope.

To find the correct amplitude of the cancellation signal, use the drive and response from the resonance measurement along with the response of the coupling. An example of the calculation is:

$$x_{cancel}(\mathrm{V}) = \frac{V_{drive,\ res.}}{V_{response,\ res.}} V_{response,\ coupling} \tag{A.1}$$

Turn up the amplitude knob of the piezo box until the zero to peak output reaches the value found with Eqn. A.1 (measured on the scope). Use the phase knob to reach either 0° or 180° phase difference between the piezo drive and the capacitive drive (measured on the scope). Manually scan the frequency across 6 Hz in .1 Hz steps. Watch the response on the lock-in. The signals on each channel will have the same height, so watching only one channel suffices. The response is not likely to be the nicely unmixed signal presented in Fig. 2.1. You will have to watch for a maximum value and a minimum value and calculate the difference between them. Systematically change the phase from one extreme to the other (0° to 180°). Flip the "invert" switch to reach the full 360° phase difference. The amplitude put out by the piezo box will change slightly as the phase is changed, so be sure to correct it every time you change the phase. Some combination of amplitude and phase driving the oscillator will result in a minimum response. Once the location of the minimum is found, explore the amplitude-phase space in the region to zero the response. Sometimes the amplitude found using Eqn. A.1 is not exactly right, and you must deviate from it to zero the oscillator motion.

Canceling the mechanical coupling vibrations is extremely difficult. It can take a few hours to get it right, and during the time the resonant frequency may drift, or something else may change. It is a good idea to periodically turn the amplitude from the piezo box down to zero and check that the coupling response has not changed. If canceling the coupling motion is extremely difficult, you may wish to also recheck the resonant response. Ideally, as long as the magnet is off, there should be zero response from the oscillator either on or off resonance. However, the degree of canceling depends on the size of the signal when the magnet is turned on. Response below 100 nV is desirable, however, Fig. 3.12 in Koki Mochizuki's dissertation [45] shows a magnet-off signal of a good 3 μV. The magnet-on signal in this figure is around 9 μV. Once you have canceled the response to something very small, take quick magnet-off and magnet-on scans and compare the two. If the magnet-off signal is much smaller than the magnet-on signal, then you are done and may go on to take data. If the magnet-off signal is close to the size of the magnet-on signal, your canceling is insufficient.

A.4.2 Taking Data

The data taking consists of five sweeps- magnet-off, magnet-on positive, magnet-off, magnet-on negative, magnet-off. The magnet-off sweeps ensure that the mechanical coupling signal remains zeroed during the data taking. The magnet-on pos/neg sweeps ensure that the signal does not depend on field direction (as it should not). These five sweeps constitute one data point. It is very difficult to get one good data point as the background signals fluctuate a lot. The coupling signal frequently changes, and the pick-up signal can change if you move a cable.

Keeping the magnet-off signal zeroed for long enough to get five good scans is probably the biggest challenge in running the experiment. If you succeed, you have reached the final step in data collection, and may go on the repeat the process at a different temperature.

A.5 Troubleshooting

If you are not getting a signal, the first things to check are the trivial ones: check for all cable connections, check that the high voltage is operating, check the drive voltage. The two real problems which are likely to occur are breakage of the oscillator and cleavage of the crystal. Both are easily identified, and both can only be fixed by opening the probe.

A.5.1 Broken Oscillator

If the problem is that the offset is outrageously high, and you cannot find a resonance signal, then the oscillator is probably broken. At room temperature, with a 10 V drive, disconnect the offset control box by removing signal input B from the lock-in. The offset on Ch. 1 should be around 12 μV. At low temperature, with 1 V drive, the offset will be about the same. If the offset is much higher than this, say, 200 μV, then the oscillator is broken. You will have to open the probe and test new oscillators.

A.5.2 Fallen or Cleaved Crystal

If the Q and resonant frequency are higher, and you get no signal with the magnet on, then the crystal has fallen off. The Q and resonant frequency drop when the crystal is attached to the oscillator. If they return to their bare oscillator values, then the crystal is indubitably gone. If the Q and resonant frequency drop dramatically, then the crystal has either cleaved or partially fallen off and is dragging against the magnet. The cure for all of these situations is to open the probe and remount the crystal.

Appendix B

Using the Photolithography Tool

The wafers are silicon, and so it is necessary to use the silicon photolithography tool. Training is essential for use of this machine. What follows is an outline of the process, but it should not be regarded as a substitute for training by a real person.

B.1 Primer Tool

Prior to using the exposure tool, the wafers must have photoresist spun on. Before the photoresist is spun on, there is a primer step. This section explains how to use the primer oven.

1) Place the wafers to be exposed into one of the Teflon holders marked "Litho". There are several of these lying about the bay.

2) Look for the orange colored oven marked "YES-3". Open the oven (after first making sure it is not in use). There is an o-ring around the oven door which frequently falls off when the oven is opened. If this happens, put it back in place before closing the oven. Set the Teflon holder with wafers inside and shut the door.

3) The black wheel-type knob should be set on 3. If it is not, turn it until it is.

Press the black “Start” button next to the wheel knob.

The primer step takes approximately 20 min. to complete. When it is done, the wafers will be very hot. Use a cloth as an oven mitt to remove the wafers from the oven. Once you have removed the wafers, press the red “Reset” key.

If no one else is using the aligner, you may set up the machine with your mask while the primer step completes. Follow all directions below up to the point where wafer mounting is described.

B.2 Exposure Tool

The components of the tool which a user must be familiar with are: the mercury exposure lamp (ultraviolet), the aligner, the microscope, and the vacuum pump.

The vacuum pump is located to the right of the tool. Turn on the vacuum before attempting to use the aligner. The mask and wafer are both held in place by vacuum.

The power supply for the mercury lamp is to the left of the tool. The mercury lamp should never be turned off. It has two settings while on: CI1 and CI2. We use glass masks, so the lamp should be set to CI2. (If using a quartz mask, the CI1 setting would be used.) The power setting is 10 mW and is set automatically upon switching to CI2.

After setting the lamp, there is a filter which must be removed. First look on the table behind the tool to see if the filter is already out. If it is not visible on the table, look for it in the machine. The filters are on the top of the machine, inside a compartment with a sliding cover. This compartment is not obvious at all, and is one of the reasons that training on the machine is indispensable. Once the compartment is located, slide the cover to the left and look down inside. The filter in question sits in the third slot from the right. If this slot is empty, then the filter has already been removed. If the filter is present, remove it and set it on a Kimwipe on the table behind the tool. (If quartz masks were used, the filter would be left in place.)

Now sign in to the tool log noting that the lamp is on CI2 and the filter has been removed.

The smaller box on the main switch box is the power supply for the microscope. The microscopes are used to align the mask with the wafer flat. Turn on the power, and also turn on the television screen to the right of the tool.

Turn on the tool with the power switch on the panel.

Now you are ready to load your mask. Generally, the tool is left with the mask holder out, ready to be loaded. If this is not the case, you will have to remove the mask holder yourself.

1) Press the “load” key. This brings all the components to the home position.

2) The (very small) LCD screen should flash the exposure time. It should say 15 s. If the exposure time is something different, press the “set exposure time” key and use the arrow keys to set the time to 15 s. Press “set exposure time” again.

3) Press the “align” key.

4) Loosen the two silver knobs on the left in order to slide out the mask holder.

5) Slide the mask holder out just a little, and wait for the microscope to move up out of the way. Then slide the mask holder out the rest of the way and rest it

upside down on the edge of the tool.

Check the size of the mask holder. We use 5 in. masks. If the mask holder is not correct, you must change it. Unscrew the vacuum connections and place the mask holder on the table behind the tool. Pick up the correct mask holder and attach the vacuum tubes to it.

Place the mask in the holder metal-side up with the horizontal alignment lines near the vacuum connections. When the holder is back in the machine and a wafer is on the aligner, the metal on the mask must be in contact with the wafer. In order to set the mask on the holder, you will first have to pull back the mechanical latch on the holder. Turn on the vacuum using the vacuum switch on the panel. Test the hold by pushing on the mask a little. It should not move. Close the mechanical latch for added security.

Replace the mask holder in the machine by turning it back right side up and sliding it into place. Tighten the two screws on the left.

Now you are ready to mount a wafer. Pull the wafer stage completely out. The wafer chuck has a set of alignment pins. There are two pins meant to align to the main wafer flat, and one pin meant to align to the secondary wafer flat. Set the wafer on the chuck photoresist-side up. I have found that for the new mask, it is best not to set the main wafer flat flush with the pins. It is better to move the wafer about .25 in. above the pins.

Push the wafer stage back in. Notice that the vacuum comes on when the stage is pushed in, and turns off only when the stage is completely out.

The silver lever on the left puts the mask in contact with the wafer. Gently pull it up until you feel resistance. The machine will beep. The mask is now in hard contact with the wafer. If at this point you wish to remove the wafer, do not press down on the lever. Instead, press the “chuck down” key on the panel. The chuck and lever will come down automatically. Frequently the lever will not go quite all the way down, and the machine will start beeping. If this happens, gently press the lever the rest of the way down.

To use the aligner, you need a soft contact rather than a hard contact. Near the large silver lever which puts the mask in hard contact is another lever with a white plastic top. This lever slides back and forth. If this lever is slid completely away from you, then the mask is in hard contact. Slide the lever towards you to raise the mask a little- this is soft contact.

The only alignment you will be concerned with is Θ alignment. We have only one mask level, so x-y alignment is not important. However, the mask features must line up with the <111> planes. The horizontal lines on the mask are for alignment to the wafer flat, thus ensuring proper plane alignment.

Use the buttons on the panel to drive around with the microscope. Observe the view on the monitor. There are two microscope lenses, left and right. You may switch the monitor from left/right split screen, to all left, to all right. The split view is best. The driving directions are reversed from what you see on the screen. Drive around for a minute or two to get used to the system.

Drive down to the bottom where the alignment features are. You may have to move the wafer a little to find the flat. The x-y translation knobs are on the microscope. Check the alignment on one end of the lines, then drive across the wafer to check it at the other end of the lines. The alignment is not likely to be off by more than a degree, so it is essential to check at both ends of the features. When the lines are aligned to the flat to your satisfaction, drive to the four corners of the pattern and make sure that the mask pattern has not fallen off the wafer. Use the x-y translation knobs to move the pattern back over the wafer, if necessary. Now slide the lever back all the way away from you to return to hard contact. You are ready to expose the wafer.

Press the "exposure" key. The machine will do the exposure, and return to a non-contact mask position. Again, the machine sometimes gets stuck, and you have to gently press the large silver lever down to a horizontal position. Pull the wafer chuck out, remove your wafer, and start on the next one.

When you have finished exposing all wafers, remove your mask from the machine by loosening the silver screws on the holder. Pull the holder out and turn it upside down to reach your mask. Turn off the vacuum on the panel. Remove your mask. The machine is generally left with the mask holder out, so you may leave it like this. Turn off the aligner, the vacuum pump, the microscope power (but not the mercury lamp!) and the monitor.

Appendix C

Using the Orange RIE

The orange RIE machine is easy to find – it is, in fact, orange. The tool has two chambers, the master and the slave chamber. You wish to use the slave chamber. This is the chamber on the right which is not in a glove box. To insure that the tool is set up for slave chamber use:

1. Turn off the RF power with the switch in between master and slave.

2. Go to the service corridor to look at the back of the tool. The rf output cable is labelled PL42. It should go in the slave chamber. Look for the gauge labelled "c.m.", located under the Main Input. There are two cables- a cable with white tape labelled PL16 and a cable with red tape also labelled PL16. The cable with **white** tape should be connected to the c.m. gauge. The vacuum pumps should be on.

3. Go back to the front of the tool. Open the large switch box on the wall to the right. Plug in PL1 and PL3A. Toggle the switches to 1 and 3A. This turns on the gasses which you want to use – 1 is freon, 3A is oxygen.

Turn the RF power back on.

4. Check the water level in the resevoir under the table. It should be full. Turn the key in the front of the machine to "slave". It should turn all the way to the

right and stop.

Now you are ready to run the RIE.

1. On the front of the tool, set the power to 333 on the display. This means 33.3% of 300 W, or 100 W. Set gas 1 (CF_4) to 62.2%, set gas 3A (O_2) to 38.8%. Log these values into the slave chamber log book.

The etch rate for this process is 1000 Å/min. The nitride is 750 Å thick. Set the timer for process 1 to .75 min. One minute may be safely used as well. Note that the RIE etches photoresist at the same rate it etches nitride.

The value of the potentiometer should be 50.0, the next switch should be on 10 V full scale, the next on Auto. The pressure should be 50 mT.

2. Open the chamber. Vent first by pressing the vent button twice. Open by holding down the toggle and pulling the joystick. The vent should be off.

Place a wafer in the chamber and close it with the toggle and joystick. Now you are going to pump down the chamber. Open the roughing pump valve which is between the two chambers. "Open" for the slave chamber means the switch points right. When the gauge on the chamber reads below -25 in Hg, close the valve (switch up is closed). Now press "pump" on the front of the tool. When the LCD gauge on the front of the tool reads 1 mT, turn off the pump. Vent to -5 in Hg on the chamber gauge. Repeat the pump down process steps, starting with the roughing pump.

After the second pump down, leave the "pump" on instead of turning it off. Then turn on in order, Auto, Gas 1, Gas 3, On.

Watch the blinking lights until the etch finishes.

3. To remove the wafer:

Turn off gas by pressing in order, Gas 1, Gas 3, On, Auto. The vent switch will be blinking. Press it twice. Turn on pump.

Go through the vent and pump down process twice to clear the chamber of all noxious gasses. Vent the chamber to the atmosphere. Open the chamber and remove the wafer.

When all wafers are etched, close the chamber and vent and pump down twice to keep it dry and under vacuum.

Bibliography

[1] H. Kamerlingh Onnes, *Akad. van Wetenschappen* **14** (1911) 818.

[2] J. G. Berdnoz and K. A. Muller, *Zeitschrift fur Physik B- Condensed Matter* **64** (1986) 189.

[3] F. and H. London, *Proc. Roy. Soc.* **A149** (1935) 71.

[4] V. L. Ginzburg and L. D. Landau, *Zh. Eksperim. i Teor. Fiz.* **20** (1950) 1064.

[5] M. Tinkham, *Introduction to Superconductivity, 2nd ed.* New York: McGraw-Hill (1996).

[6] G. Blatter et al., *Rev. Mod. Phys.* **66** (1994) 1125.

[7] M. Marder *Condensed Matter Physics* New York: John Wiley and Sons, Inc. (2000).

[8] C. Kittel *Introduction to Solid State Physics, 7th ed.* Ney York: John Wiley and Sons, Inc. (1996).

[9] J. Bardeen and M. J. Stephen, *Phys. Rev.* **140** (1965) A1197.

[10] Y. B. KIm, C. F. Hempstead, and A. R. Strnad, *Phys. Rev.* **139** (1965) A1163.

[11] P. Noziere and W. F. Vinen, *Phil. Mag.* **14** (1966) 667.

[12] A. A. Abrikosov, *Zh. Eksp. i Teor. Fiz.* **32** (1957) 1442.

[13] S. J. Hagen et al., *Phys. Rev. B* **47** (1993) 1064.

[14] C. D. Dewhurst, S. S. James, R. A. Doyle, Y. Paltiel, H. Shtrikman, E. Zeldov, D. McK. Paul, *Phys. Rev. B* **63** (2001) 1.

[15] E. B. Nyeanchi and X.-M. Zhu, *Jour. Low Temp. Phys.* **117** (1999) 1429.

[16] M. Velez, J. I. Martin, E. M. Gonzalez and J. L. Vicent, *Complex Behavior of Glassy Systems* Berlin: Springer (1997).

[17] E. B. Sonin, *Phys. Rev. B* **55** (1997) 485.

[18] D. J. van Ooijen and G. J. van Gurp, *Phys. Letters* **17** (1965) 230.

[19] N. B. Kopnin and V. E. Kratsov, *Pis'ma Zh. Eksp. Teor. Fiz.* **23** 631 [*JEPT Lett.* **23** (1976) 578].

[20] N. B. Kopnin and V. E. Kratsov, *Zh. Eksp. Teor. Fiz.* **71** 1644 [*Sov. Phys. JEPT* **44** (1976) 861].

[21] N. B. Kopnin and M. M. Salomaa, *Phys. Rev. B* **44** (1991) 9667.

[22] M. V. Feigel'man, V. B. Geshkenbein, A. I. Larkin, and V. M. Vinokur, *JEPT Lett.* **62** (1997) 834.

[23] P. Ao and D. J. Thouless *Phys. Rev. Lett.* **70** (1993) 2158.

[24] D. J. Thouless, P. Ao, and Q. Niu Phys. Rev. Lett. **76** (1996) 3758.

[25] J. T. Markert, K. Mochizuki, E. E. Judge *Physica B*, **284-288** (2000) 723.

[26] G. D'Anna, M.-O. Andre, and W. Benoit, *Europhys. Lett.* **25** (1994) 539.

[27] A. Gupta, Y. Kopelevich, M. Ziese, P. Esquinazi, P. Fischer, F. I. Schulz, and H. F. Braun, *Phys. Rev. B.* **48** (1993) 6359.

[28] L. Richard, J. Woirgard, T. Aouaroun, and J. Rabier, *Jour. Phys. IV* **6** (1996) 493.

[29] A. Barr, it Phys. Rev. Lett. **77** (1996) 731.

[30] P. L. Gammel, L. F. Schneemeyer, J. V. Waszczak, and D. J. Bishop, *Phys. Rev. Lett.* **61** (1998) 1666.

[31] D. J. Baar and J. P. Harrison, *Physica C* **157** (1989) 215.

[32] G. D'Anna and W. Benoit, *Rev. Sci. Instrum.* **61** (1990) 3821.

[33] J. Woirgard, Y. Sarrazin, and H. Chaumet, *Rev. Sci. Instrum.* **48** (1977) 1322.

[34] E. Brandt, P. Esquinazi, H. Neckel, and G. Weiss *Phys. Rev. Lett.* **56** (1986) 89.

[35] E. Brandt, *Phys. Rev. Lett.* **68** (1992) 3769.

[36] P. Esquinazi, *Jour. Low Temp. Phys.* **85** (1991) 139.

[37] M. Ziese, P. Esquinazi, and H. F. Braun, *Supercond. Sci. Technol.* **7** (1994) 869.

[38] X.-M. Zhu, E. Brandstrom and B. Sundqvist, *Phys. Rev. Lett.* **78** (1997) 122.

[39] R. N. Kleiman, G. K. Kaminsky, J. D. Reppy, R. Pindak, and D. J. Bishop *Rev. Sci. Instrum.* **56** (1985) 2088.

[40] T. T. M. Palstra et al, *Phys. Rev. B* **38** (1988) 5102.

[41] S. Martin et al, *Appl. Phys. Lett.* **54** (1989) 72.

[42] V. B. Braginsky and A. B. Manukin, *Measurement of Weak Forces in Physics Experiments* Chicago: University of Chicago Press (1977).

[43] P. G. deGennes and J. Matricon, *Rev. Mod. Phys.* **36**, (1964) 45.

[44] X. Liu, S. F. Morse, J. F. Vignola, D. M. Photiadis, A. Sarkissian, M. H. Marcus, and B. H. Houston, *App. Phys. Lett.* **78** (2001) 1346.

[45] K. Mochizuki, PhD. dissertation University of Texas (1998).

[46] S. D. Timoshenko and J. N. Goodier, *Theory of Elasticity* New York: McGraw-Hill (1970).

[47] W. C. Young, *Roark's Formulas for Stress and Strain* New York: McGraw-Hill (1989).

[48] K. Mochizuki, private comments.

[49] S. K. Ghandhi, *VLSI Fabrication Principles Silicon and Gallium Arsenide, 2nd ed.* New York: John Wiley and Sons, Inc. (1994).

[50] J. P. Zhou, D. R. Riley, A. Manthiram, M. Arendt, M. Schmerling, and J. T. McDevitt, *Appl. Phys. Lett.* **4** (1993) 548.

[51] M. F. Yan, R. L. Barns, H. M. O'Bryan, Jr., P. K. Gallagher, R. C. Sherwood, and S. Jin, *Appl. Phys. Lett.* **51** (1987) 532.

[52] J. P. Zhou, D. R. Riley, J. T. McDevitt, *Chem. Mater.* **5** (1993) 361.

[53] J. P. Zhou and J. T. McDevitt, *Solid State Commun.* **86** (1993) 11.

[54] J. P. Zhou, S. M. Savoy, J. Zhao, D. R. Riley, Y. T. Zhu, A. Manthiram, R. K. Lo, D. Borich, and J. T. McDevitt, *J. Amer. Chem. Soc.* **116** (1994) 9389.

[55] J. P. Zhou, S. M. Savoy, R. K. Lo, J. Zhao, M. Arendt, Y. T. Zhu, A. Manthiram, and J. T. McDevitt, *Appl. Phys. Lett.* **66** (1995) 2900.

[56] I. D. Brown, J. Solid State Chem. 90 (1991) 1952.

[57] Q. Huang, R. J. Cava, A. Santoro, J. J. Krajewski, and W. F. Peck, *Physica C* **193** (1992) 196.

[58] A. Manthiram and J. B. Goodenough, *Physica C* **159** (1989) 760.

Vita

Elizabeth Eileen Judge was born March 23, 1971. She attended high school at St. Brendan High School in Miami, FL. She attended the Pennsylvania State University from 1989 to 1990. She attended the State University of New York at Stony Brook from 1991 to 1995, graduating with a B.S. in Physics and Astronomy. She came to the University of Texas at Austin in 1995.

Permanent address: 610 W. 30th St. #201, Austin TX, 78705.

This dissertation was typed by the author.